X

NASA Technical Memorandum 85760

Wind-Tunnel Investigation of an Advanced General Aviation Canard Configuration

Joseph R. Chambers, Long P. Yip,
and Thomas M. Moul

APRIL 1984

NASA

NASA Technical Memorandum 85760

Wind-Tunnel Investigation of an Advanced General Aviation Canard Configuration

Joseph R. Chambers, Long P. Yip,
and Thomas M. Moul
Langley Research Center
Hampton, Virginia

National Aeronautics
and Space Administration

**Scientific and Technical
Information Office**

1984

SUMMARY

Wind-tunnel tests of a model of an advanced general aviation canard configuration were conducted in the Langley 30- by 60-Foot Tunnel. The objective of the tests was to determine the aerodynamic stability and control characteristics of the configuration for a large range of angles of attack and sideslip for several power conditions.

For forward center-of-gravity locations, the model did not exhibit any stability and control characteristics which would be viewed as unsafe. The results also indicate that the configuration would be extremely stall resistant. This highly desirable stall-resistance characteristic resulted from the fact that the canard was designed to stall prior to the wing. Stalling of the canard resulted in increased longitudinal stability and decreased elevator effectiveness; both effects limited the maximum obtainable trim angle of attack to values below those required for wing stall for all power conditions tested.

For aft center-of-gravity locations and high-power, low-speed conditions, the combined effects of nose-up trim changes due to power and reduced longitudinal stability overpowered the stall resistance provided by the canard. Large nose-up elevator control inputs in this condition could result in stalling of the wing. Wing stall results in longitudinal instability and large nose-up moments which would tend to increase angle of attack to a high-angle-of-attack, deep-stall trim condition. The configuration had insufficient elevator effectiveness for recovery from the high-power deep-stall condition. Both a reduction in power and use of nose-down elevator were required for recovery.

Lateral-directional stability and control characteristics were degraded at wing-stall and post-stall angles of attack. In particular, the dihedral effect became unstable at stall, large directional trim changes occurred at high power settings, and the rudder and aileron effectiveness became negligible at angles of attack associated with the deep-stall condition.

The wind-tunnel results also indicate a marked reduction in longitudinal stability at negative angles of attack because of increased aerodynamic interference between the canard and the wing. Although the elevator remained effective for this condition, the loss of longitudinal stability (particularly for aft center-of-gravity locations) is undesirable.

INTRODUCTION

Wind-tunnel tests of a 1/3-scale model of an advanced canard-configured general aviation airplane were conducted at the NASA Langley Research Center. An extensive test program was accomplished for a large range of angles of attack, angles of sideslip, and power conditions. Flow-visualization tests were also conducted to aid in the interpretation and analysis of aerodynamic characteristics. The information presented herein is a summary of the more pertinent results and conclusions obtained during the tests.

SYMBOLS

All longitudinal forces and moments are referred to the wind-axis system, and all lateral-directional forces and moments are referred to the body-axis system. Moment data are presented for a forward center-of-gravity position of fuselage station 23.3 in. (-73 percent of the reference mean aerodynamic chord) and for an "aft" center-of-gravity position of fuselage station 24.8 in. (-63 percent of the reference mean aerodynamic chord). The center of gravity was located on the thrust axis to eliminate any moments due to the thrust moment arm. Dimensional quantities are presented in U.S. Customary Units.

b wing span, ft

C_L configuration lift coefficient, $\frac{\text{Lift}}{q_\infty S}$

$C_{L,c}$ lift coefficient of canard, $\frac{\text{Canard lift}}{q_\infty S_c}$

$C_{L,w}$ lift coefficient of wing, $\frac{\text{Wing lift}}{q_\infty S}$

C_l rolling-moment coefficient, $\frac{\text{Rolling moment}}{q_\infty Sb}$

C_{l_β} $= \frac{\partial C_l}{\partial \beta}$

C_m pitching-moment coefficient, $\frac{\text{Pitching moment}}{q_\infty S\bar{c}}$

C_N normal-force coefficient, $\frac{\text{Normal force}}{q_\infty S}$

C_n yawing-moment coefficient, $\frac{\text{Yawing moment}}{q_\infty Sb}$

C_{n_β} $= \frac{\partial C_n}{\partial \beta}$

C_T thrust coefficient, $\frac{\text{Thrust}}{q_\infty S}$

$\bar{c}$ mean aerodynamic chord, in.

F_c normal force of canard, lbf

F_p normal force of propeller, lbf

F_w normal force of wing, lbf

q_∞ free-stream dynamic pressure, lbf/ft^2

S reference wing area, ft^2

S_c exposed planform area of canard, ft^2

α angle of attack, deg

β angle of sideslip, deg

δ_e deflection angle of elevator, positive for trailing edge down, deg

Abbreviations:

BL butt line, in.

c.g. center of gravity

FS fuselage station, in.

L.E. leading edge

WL water line, in.

DESCRIPTION OF MODEL

A three-view sketch of the 1/3-scale model is presented in figure 1, photographs of the model are shown in figure 2, and geometric characteristics of the model are listed in table I. The design incorporated a close-coupled, fixed canard and an aft-mounted wing of relatively low sweep. A single-slotted flap (referred to herein as the elevator) on the canard provided pitch control, inboard wing-mounted ailerons provided roll control, and a conventional rudder provided yaw control.

The model was constructed primarily of wood with a fiberglass outer skin. Power for the propeller was provided by a tip-turbine air motor driven by compressed air. Aerodynamic characteristics of the complete model were measured with a conventional six-component strain-gage balance that was internally mounted. In addition, auxiliary balances were used to measure the individual aerodynamic contributions of the canard and of the outer right wing panel. The canard spar and the carry-through structure were mounted directly to a strain-gage balance in the fuselage nose section. The right wing was constructed of separate inner and outer panels, and the outer panel was mounted to a strain-gage balance located within the inner wing-panel structure. The gap between the inner and outer wing panels was sealed with flexible tape.

The tests were conducted in the Langley 30- by 60-Foot Tunnel. As shown in figure 3, the model and its internal strain-gage balances were mounted to a motorized sting assembly which was remotely actuated to travel along a curved strut for variations in the model angle of attack. The variations in angle of sideslip were provided by a second remotely actuated motor which rotated the base of the curved strut about a vertical axis. As shown in figure 3, compressed air for the air motor was provided by flexible plastic hoses, which trailed behind the sting assembly during tests.

The tests were conducted for a range of angles of attack of -28° to 92° and for a range of angles of sideslip of ±15°. Besides longitudinal and lateral-directional force and moment tests, control effectiveness tests and component build-up tests (to identify aerodynamic contributions of individual airframe components and aerodynamic

interference effects) were conducted. In addition, wool tufts were used in flow-visualization tests to define airflow characteristics over the model.

The test program was conducted at a wind-tunnel airspeed of 69 ft/sec, which resulted in a dynamic pressure of 5.6 lbf/ft^2 and a Reynolds number of 0.55×10^6 based on the mean aerodynamic chord of the wing. In view of the relatively low value of test Reynolds number, the reader is cautioned that the aerodynamic characteristics of a full-scale airplane may be different than those of the present model because of Reynolds number effects. All aerodynamic data have been based on the geometric characteristics of the wing.

STALL CHARACTERISTICS OF CANARD CONFIGURATIONS

The results of the wind-tunnel test indicate that the stability and control characteristics of the model were generally satisfactory for the low angles of attack representative of cruise conditions. However, the stall and post-stall characteristics of the configuration varied from highly desirable to undesirable, depending on center-of-gravity location and power condition. Prior to discussion of these results, a brief review of some fundamental principles of design for satisfactory stall characteristics of canard airplanes will provide background to aid in interpretation of the data and discussion.

Shown in figure 4 are wind-tunnel data (ref. 1) measured in the Langley 30- by 60-Foot Tunnel for a pusher canard-airplane design known to be very stall resistant on the basis of flight experience. In figure 4(a), the variations of lift coefficient C_L and pitching-moment coefficient C_m with angle of attack α are presented for the elevator fixed at a maximum nose-up deflection angle. The lift curve shows two distinct breaks. The first break, which occurs near $\alpha = 11°$, resulted from stalling of the canard surface, which was designed to stall prior to the wing. The second lift break occurs near $\alpha = 24°$ and is indicative of wing stall.

The inherent angle-of-attack-limiting characteristic of the foregoing stall sequence is illustrated by the pitching-moment data. The configuration is longitudinally stable for angles of attack from 0° to 10°, since the slope $dC_m/d\alpha$ is negative. As expected, the maximum elevator deflection produces large nose-up values of C_m at low angles of attack; however, as angle of attack is increased to 11°, the previously mentioned canard stall is encountered, resulting in an incremental loss of canard lift with further increases in angle of attack. The stabilizing lift contribution of the unstalled wing then dominates, and therefore the configuration experiences a marked increase in stability, as shown by the pronounced increase in negative slope of C_m near $\alpha = 14°$ in figure 4(a). The maximum obtainable trim angle of attack is limited to about 16°, well below the value of 24° required for wing stall.

In addition to the increase in stability provided by canard stall, the phenomenon also results in decreased elevator effectiveness, since stalled flow also exists on the canard-mounted elevator. Therefore, as shown in figure 4(b), the elevator deflection required for trim at high angles of attack increases significantly, and wing stall cannot be induced for maximum elevator input.

The effectiveness of this highly desirable stall-resistance characteristic provided by the canard configuration concept can be influenced by many design variables, including airfoils and relative geometry of the canard and wing, propeller location, and center-of-gravity location. The effects of these variables must be accounted for in order to ensure that the wing cannot be stalled; in addition, the airplane must be

recoverable from excursions at high angles of attack generated by special maneuvers such as tail-slide maneuvers or zoom stalls to zero airspeed.

RESULTS OF FLOW-VISUALIZATION TESTS

Flow-visualization and force tests made with the model of this investigation indicated that the configuration complied with the basic principle of canard airplane design in that the canard stalled before the wing. Results of wool tuft flow-visualization tests conducted to analyze stall behavior of the canard and wing surfaces are presented in figure 5. The photographs, which were taken from a rear overhead position, illustrate the flow over the model for neutral controls with the propeller windmilling. The photographs are presented for a range of angles of attack from 0° to 28°.

For $\alpha = 0°$ (fig. 5(a)), which corresponds to cruise conditions, the flow was attached over the canard and wing surfaces. When the angle of attack was increased to 6° (fig. 5(b)), flow separation occurred at the canard-fuselage juncture. The separated-flow region increased in a spanwise direction for $\alpha = 10°$ (fig. 5(c)). When the angle of attack was increased to 12° (fig. 5(d)), the flow over the left canard surface stalled abruptly, followed by a similar abrupt stall of the right canard surface at $\alpha = 14°$ (fig. 5(e)). Also apparent at $\alpha = 14°$ was the onset of trailing-edge separation on the wing. At $\alpha = 16°$ (fig. 5(f)), the wing trailing-edge separation increased, and at $\alpha = 18°$ (fig. 5(g)), the outer wing panels of the wing stalled abruptly. For $\alpha = 22°$ (fig. 5(h)), the outer wing panels were stalled, as was the canard. The tufts indicated attached flow on the canard elevator as a result of flow through the slotted elevator. The downwash from the canard resulted in a significant reduction in local angle of attack on the inner wing panels and, therefore, the flow on the inner wing panels remained attached up to high angles of attack.

Shown in figure 6 are photographs which illustrate the effects of power on stall patterns at $\alpha = 28°$. Figure 6(a) shows flow over the model for the windmilling propeller condition, indicating stalled wing and canard surfaces with small areas of attached flow on the inboard leading edge of the wing and slot flow over the canard elevator. The effects of power on the flow patterns are illustrated by conditions for a thrust coefficient C_T of 0.4, which is a value that corresponds to a high-power, low-speed condition. For $C_T = 0.4$ (fig. 6(b)), the slipstream of the tractor propeller significantly affected the flow over the right inboard canard and wing surfaces. The previously noted separated flow at the canard-fuselage juncture became attached, and the attached flow area on the inner right wing panel was increased. The left canard and wing showed little effect of power, suggesting that the propeller slipstream swirl may have caused the asymmetry effects by decreasing the local angle of attack on the inboard right side of the model.

Flow-visualization tests made for the elevator deflections other than 0° and analysis of force and moment data indicated an effect of elevator angle on canard stall characteristics. For example, as elevator deflection was increased to the maximum value of 35°, the stall angle of attack of the canard decreased by about 5° and the canard stall was more abrupt.

As discussed subsequently, the relative angles of attack for onset of stall for the canard and the wing, the relatively abrupt stall of both surfaces, and the effect of power on the stall progression all had significant effects on the stall resistance of the configuration.

LONGITUDINAL CHARACTERISTICS FOR FORWARD CENTER-OF-GRAVITY LOCATIONS

The overall static longitudinal stability and control characteristics of the model for forward center-of-gravity locations were satisfactory. In addition, the results indicate a high degree of stall resistance, in accordance with the highly desirable nature of canard configurations as previously discussed. A center-of-gravity location of FS 23.3 in. was chosen for this phase of the tests.

The lift, drag, and pitching-moment characteristics obtained for this forward center-of-gravity location are presented for power-off conditions in figure 7. The variation of lift coefficient with angle of attack is characterized by the two distinct breaks previously discussed for typical canard configurations. As shown by the flow-visualization tests (fig. 5), canard stall occurred at $\alpha = 12°$ for $\delta_e = 0°$, and the canard stall angle decreased to $\alpha = 7°$ for $\delta_e = 35°$. Maximum lift and wing stall occurred near $\alpha = 18°$, also in agreement with observations made during the flow-visualization studies previously discussed.

The pitching-moment data of figure 7 indicate that the longitudinal stability of the model increased markedly as the canard stalled, as would be expected of a canard configuration. Canard stall also resulted in an extremely large loss of elevator effectiveness. The combined effects of increased stability and decreased control effectiveness resulted in a maximum value of trimmed angle of attack of about 11° for $\delta_e = 35°$ and $C_L = 1.3$.

Inspection of the data of figure 7 reveals a region of longitudinal instability (positive values of $dC_m/d\alpha$) for angles of attack from 18° to 35°. This unstable region was of no concern for this center-of-gravity location, however, inasmuch as large nose-down values of pitching-moment coefficient existed for that range of angles of attack. These nose-down moments would cause the angle of attack to reduce to the trimmed value of 11° for $\delta_e = 35°$ if the configuration was perturbed to angles in excess of 11° by dynamic control inputs, wind gusts, and so forth.

Thus, the configuration was inherently stall resistant for this representative forward center-of-gravity position. The stall-resistance characteristic is depicted in figure 8, which presents values of elevator deflection angle required to trim the model to various angles of attack. For power-off conditions, the data trends are very similar to those previously discussed for the stall-resistant configuration in figure 4; that is, the elevator deflection angle required to increase angle of attack markedly increased when the canard stalled, and angle of attack was inherently limited to values below that required for wing stall. The data of figure 8 also indicate that a high-power, low-speed condition of $C_T = 0.4$ resulted in a reduction in longitudinal stability prior to canard stall; however, the maximum obtainable angle of attack was still limited to about 12°.

In summary, the wind-tunnel results indicate that the model exhibited no critical longitudinal stability and control deficiencies for a forward center-of-gravity position. The results indicate a highly desirable stall-resistant behavior, with recovery possible from high-angle-of-attack excursions.

LONGITUDINAL CHARACTERISTICS FOR AFT CENTER-OF-GRAVITY LOCATIONS

In contrast to the highly desirable stall-resistant behavior exhibited by the model for forward center-of-gravity locations, a marked degradation in stall resistance, stability at the stall, and post-stall recovery occurred for aft center-of-

gravity locations. In order to illustrate these points, the foregoing wind-tunnel data have been recomputed and referred to a more rearward center-of-gravity location of FS 24.8 in. Inasmuch as variations in center-of-gravity location do not affect lift or drag characteristics, the effects are discussed in terms of variations in pitching moment and in longitudinal stability and control.

Presented in figure 9 are the values of pitching-moment coefficient referred to FS 24.8 in. for power-off conditions. As a result of the normal reduction in longitudinal stability caused by rearward movement of the center of gravity, the magnitudes of nose-down moments at post-stall angles of attack were markedly reduced. For $\delta_e = 35°$, the maximum trimmed angle of attack remained at 12° as for the forward center-of-gravity condition; however, a second stable trim point existed at $\alpha = 41°$. Nose-down elevator deflection ($\delta_e = -20°$) provided the negative values of pitching-moment coefficient required for recovery from the post-stall trim condition.

In addition to the degrading effects of the aft center-of-gravity location on post-stall recovery moments, further reductions in stall resistance and post-stall recovery resulted from power effects. The effects of thrust on pitching-moment coefficient are presented in figure 10 for $\delta_e = 35°$. For $C_T = 0.4$, large nose-up trim changes were apparent which further reduced the angle-of-attack-limiting characteristics of the canard to the extent that the maximum trim value of angle of attack could have exceeded that required for wing stall. The nose-up moments produced by $\delta_e = 35°$ near $\alpha = 18°$ could have resulted in wing stall and entry into a region of longitudinal instability with a stable "deep-stall" trim point near $\alpha = 60°$. Recovery from the deep-stall condition requires nose-down moments near $\alpha = 60°$. As indicated in figure 11, full nose-down control ($\delta_e = -20°$) at $\alpha = 60°$ did produce negative values of pitching-moment coefficient. However, as angle of attack was reduced during the recovery attempt, the magnitude of the pitching-moment coefficient was reduced. At $\alpha = 50°$ the recovery moment became zero, resulting in another deep-stall trim condition. Recovery from deep stall was possible if power was reduced to idle.

An indication of the powerful influence of center-of-gravity location on recovery from the deep-stall condition for this configuration is presented in figure 12. Figure 12 is the variation of pitching-moment coefficient with normal-force coefficient C_N for $C_T = 0.4$ and for a full nose-down elevator deflection $\delta_e = -20°$. Also plotted are radial lines which represent $C_m = 0$ for various center-of-gravity locations. Recovery from the deep-stall condition requires that negative values of pitching-moment coefficient be produced by $\delta_e = -20°$. As indicated by the data, recovery was possible for center-of-gravity locations forward of about FS 24.7 in. For center-of-gravity locations at and aft of FS 24.7 in., however, recovery from the high-power deep stall by using only elevator control became marginal.

The effects of the aft center-of-gravity, high-power condition on elevator deflection angle required for trim are shown in figure 13. As indicated by the data, elevator deflections resulted in angles of attack in excess of the wing-stall angle of attack for center-of-gravity locations of FS 24.8 in. and FS 25.7 in., followed by trim at extremely high angles of attack.

LONGITUDINAL CHARACTERISTICS AT NEGATIVE ANGLES OF ATTACK

In addition to the foregoing characteristics, the model also exhibited a marked reduction in longitudinal stability at negative angles of attack. As shown in figure 14, the stability reduction for FS 24.8 in. was large enough to result in neutral

to unstable characteristics. Analysis of individual canard and wing-body contributions to longitudinal stability indicate the loss of stability was caused by a pronounced increase in adverse aerodynamic interference between the canard and the wing for negative angles of attack. In particular, the data show that the lift-curve slope of the wing was significantly reduced at negative angles of attack because of increased downwash from the canard. The stabilizing contribution of the wing to longitudinal stability was, therefore, reduced and overpowered by the destabilizing contribution of the canard, resulting in marginal longitudinal stability.

As shown in figure 15, the elevator effectiveness at negative angles of attack for FS 24.8 in. was maintained. However, controllability of the configuration would be degraded, and such characteristics are unconventional and undesirable.

LATERAL-DIRECTIONAL CHARACTERISTICS

The wind-tunnel data indicate that the lateral-directional stability and control characteristics of the model were satisfactory for normal flight operations at angles of attack below wing stall. Within this range of angles of attack, the model exhibited positive directional stability, stable dihedral effect, and satisfactory aileron and rudder effectiveness for forward and aft center-of-gravity locations. For angles of attack near or greater than the value required for wing stall, however, several degraded lateral-directional characteristics were exhibited which would affect the controllability of the model, particularly in combination with the unconventional longitudinal behavior previously noted for high-power, aft center-of-gravity conditions.

Shown in figure 16 are the variations of yawing-moment coefficient C_n with angle of attack for full rudder deflections at zero sideslip and $C_T = 0.4$. The data indicate that a large nose-left yawing moment was produced at the high-power, low-speed condition. This effect, which was probably caused by swirl of the propeller slipstream, required a large nose-right rudder deflection for directional trim at angles of attack near wing stall ($\alpha = 18°$). For higher angles of attack, the rudder effectiveness was rapidly reduced because of impingement of the low-energy, stalled wing wake on the vertical tail and geometric alignment of the rudder hinge line in a direction almost parallel to the free-stream velocity. The data indicate that directional control under high-power condition would be marginal near $\alpha = 25°$.

Rolling-moment coefficients produced by the ailerons are presented in figure 17. The data indicate that a roll asymmetry to the left occurred, and that asymmetry could not be controlled above $\alpha = 22°$. In addition, the aileron effectiveness decreased markedly for post-stall angles of attack because of wing stall and flow separation over the inboard-mounted ailerons. The foregoing data indicate the lateral-directional controllability of the configuration would be markedly reduced at post-stall angles of attack, particularly at angles near the high-power, deep-stall trim condition ($\alpha = 60°$).

In addition to reduced control effectiveness, the configuration exhibited unstable lateral and directional stability at post-stall angles of attack. Shown in figure 18 is the variation of the directional-stability derivative C_{n_β} with angle of attack for $C_T = 0.4$. The data show a large reduction in C_{n_β} at angles of attack greater than wing stall such that the configuration became directionally unstable at $\alpha \geq 30°$. The loss of directional stability at post-stall angles of attack was caused by impingement of the low-energy stalled wake on the vertical tail. As shown in figure 19, the lateral-stability derivative C_{l_β} was strongly affected by elevator

deflection. The loss of lateral stability was caused by asymmetric wing stall under sideslip conditions. (The advancing wing stalled prior to the retreating wing.) Elevator deflection aggravated the asymmetric stall because the canard downwash reduced the local angle of attack on the retreating wing in the sideslip condition, thereby delaying stall on the retreating wing and causing the advancing wing to stall first.

CONFIGURATION EFFECTS ON STALL RESISTANCE

As part of the present investigation, an attempt was made to identify the configuration features of the model which resulted in the foregoing undesirable stall and post-stall characteristics for high-power, aft center-of-gravity conditions. As indicated by the results of flow-visualization tests and force tests, the configuration experienced canard stall prior to wing stall in accordance with design principles for canard configurations. However, the results of the present investigation indicate that certain adverse configuration-dependent effects can overpower the stall resistance provided by the canard. The degrading effects of aft center-of-gravity locations have already been discussed; however, several geometric features can also have significant effects on stall resistance.

A particularly informative illustration of configuration effects for canard-airplane designs was provided by comparison of the present wind-tunnel results with wind-tunnel data (ref. 1) previously obtained for the stall-resistant pusher canard airplane discussed in a previous section. Shown in figure 20 is a comparison of pitching-moment coefficients for the two configurations for power-off conditions and neutral controls. Of particular interest is the region near wing stall for both designs. The data for the present model indicate longitudinal instability from $\alpha = 18°$ (wing stall) to $\alpha = 32°$ and minimal nose-down moments at high angles of attack, whereas data for the stall-resistant pusher configuration indicate approximately neutral stability and large nose-down moments at high angles of attack. These different post-stall aerodynamic characteristics, which are extremely significant for stall resistance, are affected to a large extent by the stalling characteristics of the airfoils selected for the canard and wing.

Shown in figure 21 are the lift contributions of the isolated canards (as measured by a canard balance) for each configuration. The pusher configuration uses the GU 25-5(11)8 airfoil section (ref. 2), and the present design uses the NACA 23018 section. Significant differences can be noted in the general stall characteristics of the canards. In particular, data for the canard of the pusher configuration indicate a relatively gentle trailing-edge stall near $\alpha = 11°$, with approximately constant lift as angle of attack is increased to $\alpha = 23°$; data for the present model indicate a relatively abrupt stall near $\alpha = 8°$, with a post-stall increase in lift-curve slope. These variations in lift characteristics result in significant changes in the contributions of the canard to longitudinal stability at high angles of attack.

It should be noted that the canard and wing contributions to stability are generally related to lift-curve slopes and are of an opposite nature; that is, a positive lift-curve slope for the forward-mounted canard is destabilizing (positive contribution to $dC_m/d\alpha$), whereas a positive lift-curve slope for the wing-body combination is stabilizing (negative contribution to $dC_m/d\alpha$). Likewise, negative lift-curve slopes are stabilizing for the canard and destabilizing for the wing-body combination. The difference between the canard and the wing-body contributions, with additional interference factors, represents the longitudinal stability of the total

airplane. The angle of attack for wing stall is indicated for each configuration, and it is interesting to examine the canard contribution to stability in the immediate vicinity of wing stall. Thus, the data indicate that the canard of the present model contributes destabilizing moments whereas the canard of the pusher configuration contributes stabilizing moments. At immediate post-stall angles of attack, the lift-curve slope of the wing for both configurations is negative, indicating destabilizing contributions. When the destabilizing contributions of the canard and the wing are combined for the present model, the complete configuration exhibits the instability shown in figure 20. However, the stabilizing canard and destabilizing wing contributions for the pusher configuration offset one another, resulting in near neutral stability. In summary, the airfoil selected for the canard of the present model exhibited undesirable lift characteristics at angles of attack beyond canard stall.

Finally, the significance of the critical power effects noted for the model can be illustrated by comparison with those of the pusher configuration in figures 22 and 23. Shown in figure 22 are sketches which illustrate the major effects of power. For the present model, analysis of the wind-tunnel data indicates that the large nose-up trim changes previously discussed were caused by a combination of direct propeller force contributions and induced effects. The direct propeller contribution was the propeller normal force, or "fin effect," which caused a nose-up moment for the tractor arrangement. The effects induced by the propeller slipstream include increased canard lift and increased downwash on the wing. All these effects tended to decrease stability and to increase nose-up moments. In contrast to these results, the contribution of the pusher propeller increased stability and nose-down moments. These effects were caused by a higher thrust line and a stabilizing propeller fin effect due to the rear-mounted propeller. As shown in figure 23, the trim changes due to power for these canard airplane configurations were in opposite directions, and the stabilizing, nose-down effects of power for the pusher configuration are apparent.

CONCLUSIONS

Analysis of aerodyamic data obtained in a wind-tunnel investigation of a 1/3-scale model of an advanced general aviation canard configuration indicates the following conclusions:

1. For forward center-of-gravity locations, the model did not exhibit any stability and control characteristics which would be viewed as unsafe. The results also indicate that the configuration would be extremely stall resistant. This highly desirable stall-resistance characteristic resulted from the fact that the canard was designed to stall prior to the wing. Stalling of the canard resulted in increased longitudinal stability and decreased elevator effectiveness; both effects limited the maximum obtainable trim angle of attack to values below those required for wing stall for all power conditions tested.

2. For aft center-of-gravity locations and high-power, low-speed conditions, the combined effects of nose-up trim changes due to power and reduced longitudinal stability overpowered the stall resistance provided by the canard. Large nose-up elevator control inputs in this condition could result in stalling of the wing. Wing stall results in longitudinal instability and large nose-up moments which would tend to increase angle of attack to a high-angle-of-attack, deep-stall trim condition. The configuration had insufficient elevator effectiveness for recovery from the high-power deep-stall condition, but recovery was possible if power was reduced to idle.

3. Lateral-directional stability and control characteristics were degraded at wing-stall and post-stall angles of attack. In particular, the dihedral effect became unstable at stall, large directional trim changes occurred at high power settings, and the rudder and aileron effectiveness became negligible at angles of attack associated with the deep-stall condition.

4. The wind-tunnel results also indicate a marked reduction in longitudinal stability at negative angles of attack because of increased aerodynamic interference between the canard and the wing. Although the elevator remained effective for this configuration, the loss of longitudinal stability (particularly for aft center-of-gravity locations) is undesirable.

Langley Research Center
National Aeronautics and Space Administration
Hampton, VA 23665
March 19, 1984

REFERENCES

1. Yip, Long P.; and Coy, Paul F.: Wind-Tunnel Investigation of a Full-Scale Canard-Configured General Aviation Aircraft. ICAS Paper No. 82-6.8.2, August 1982.

2. Kelling, F. H.: Experimental Investigation of a High-Lift Low-Drag Aerofoil. C.P. No. 1187, British A.R.C., 1971.

TABLE I.- GEOMETRIC CHARACTERISTICS OF THE MODEL

Reference dimensions:	
Wing area, ft^2	10.2
Span, ft	8.44
Mean aerodynamic chord, in.	15.04
Wing:	
Area, ft^2	10.2
Span, ft	8.44
$\bar{c}$, in.	15.04
L.E. FS of $\bar{c}$, in.	34.30
Root chord, centerline, in.	19.33
Height WL, in.	4.7
Tip chord, in.	9.67
Dihedral, deg	3.0
L.E. sweep, deg	10.8
Incidence at BL 24 (airplane), relative to WL, deg	0.8
Tip incidence, relative to WL, deg	-1.2
Airfoil section:	
Root (BL 24)	NACA 23018
Tip	NACA 23012
Aileron:	
Travel, deg	-20 to 20
Chord, in.	2.67
Span, in.	21.33
Canard:	
Area, ft^2	4.97
Span, ft	6.39
$\bar{c}$, in.	9.35
L.E. FS of $\bar{c}$, in.	7.66
Root chord, in.	10.67
Height WL, in.	8.0
Tip chord, in.	8.0
Dihedral, deg	3.0
L.E. sweep, deg	0
Root incidence, relative to WL, deg	4.8
Tip incidence, relative to WL, deg	4.8
Airfoil section:	
Root	NACA 23018
Tip	NACA 23015
Elevator:	
Travel, deg	-20 to 35
Hinge line	0.76c
Vertical tail:	
Area, ft^2	1.11
Span, in.	15.0
Root chord, in.	14.67
Tip chord, in.	6.67
Airfoil section:	
Root	NACA 0012
Tip	NACA 0010.5
Rudder hinge line	0.7c
L.E. sweep, deg	45.0

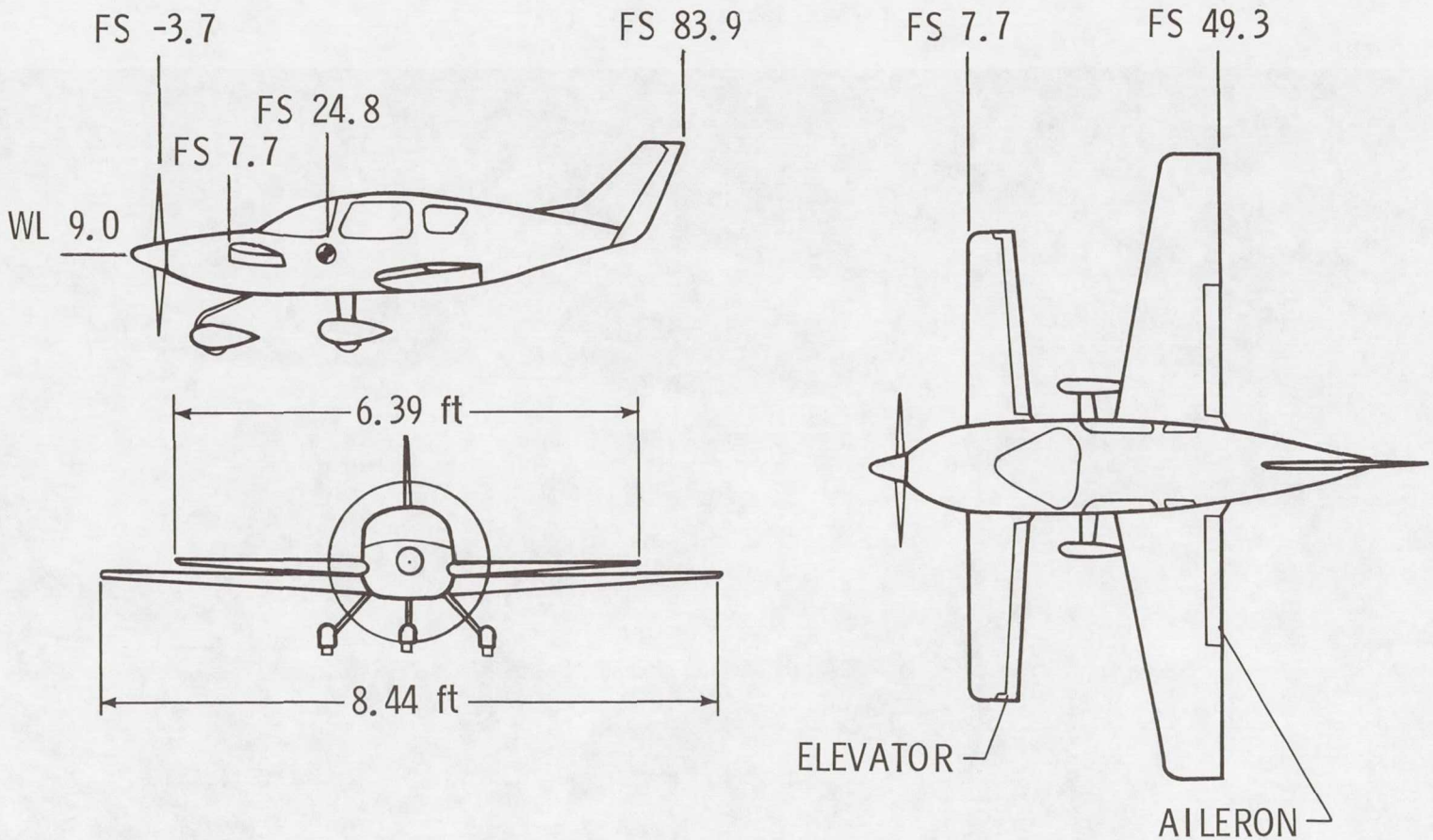

Figure 1.- Three-view sketch of model.

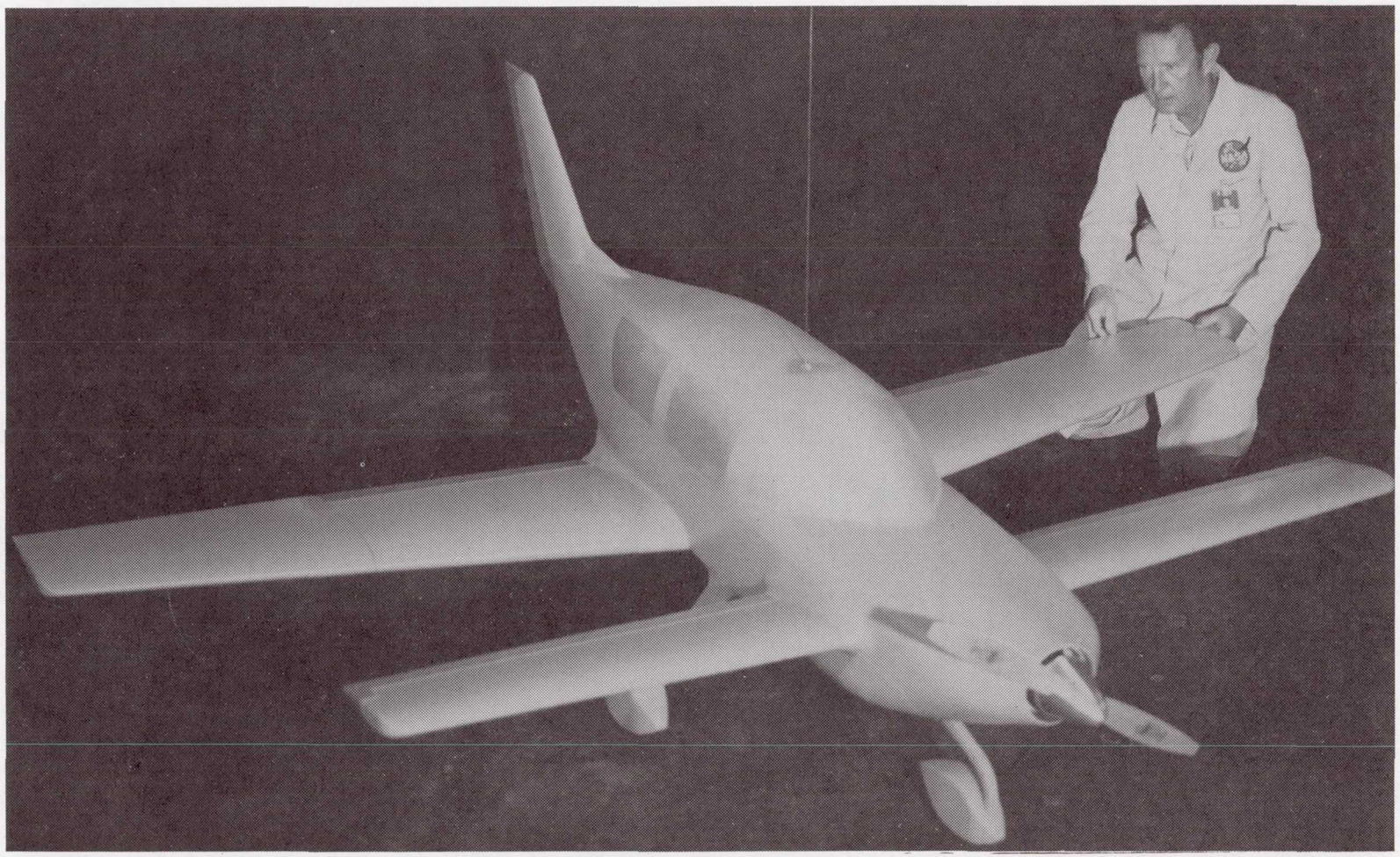

L-82-6313

(a) Front quarter view.

Figure 2.- Photographs of model.

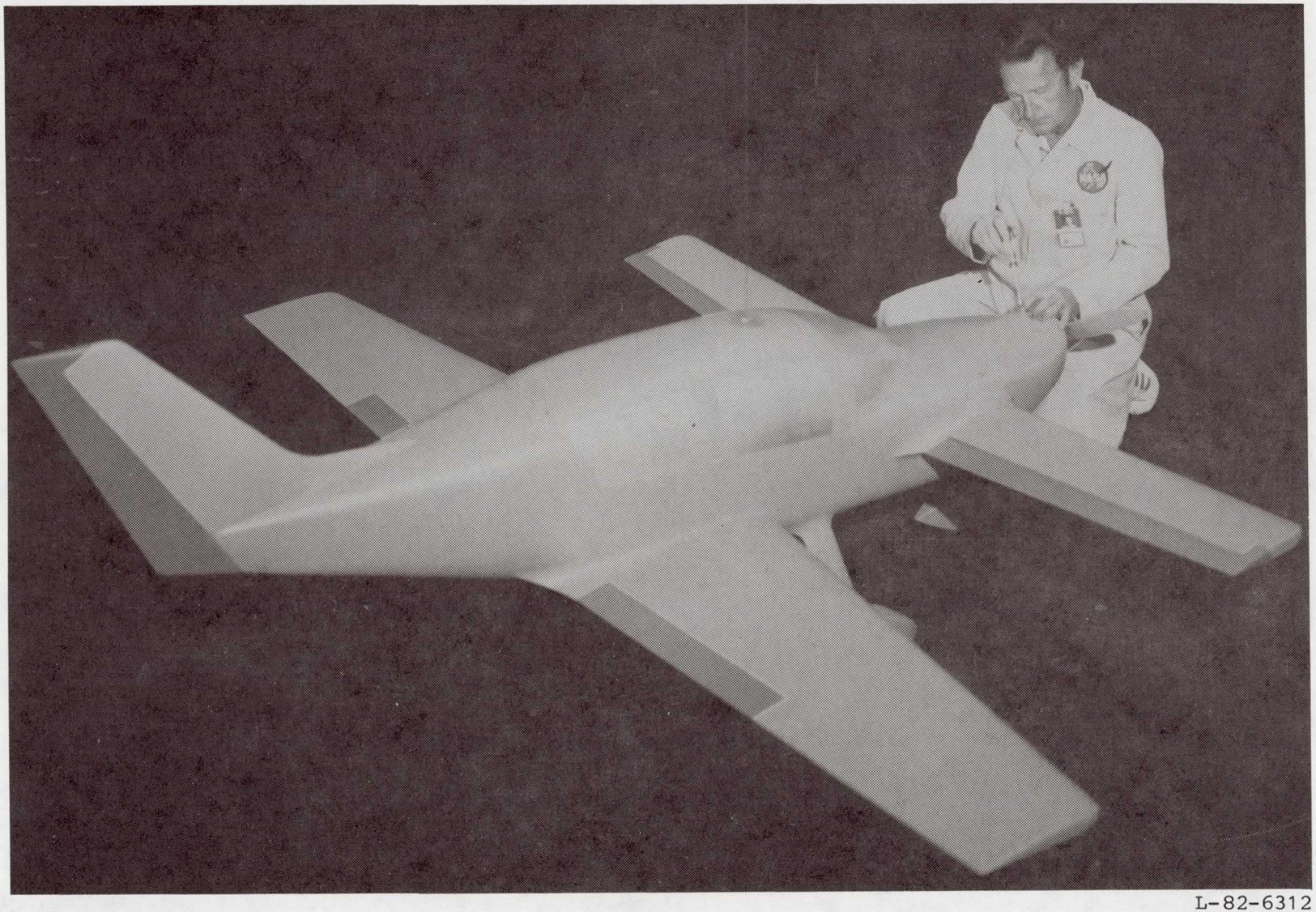

L-82-6312

(b) Rear quarter view.

Figure 2.- Concluded.

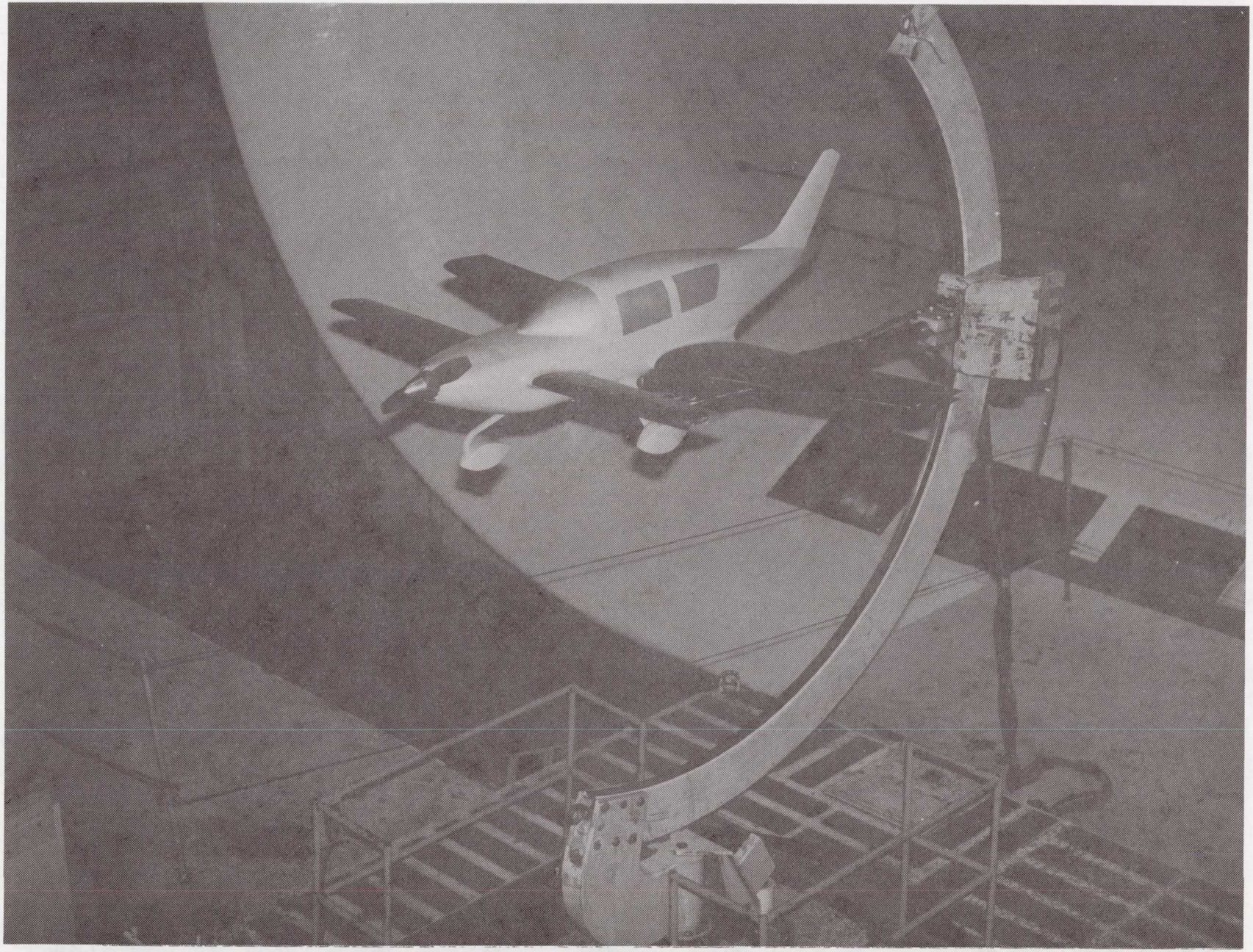

L-82-10,445

Figure 3.- Model mounted for test in Langley 30- by 60-Foot Tunnel.

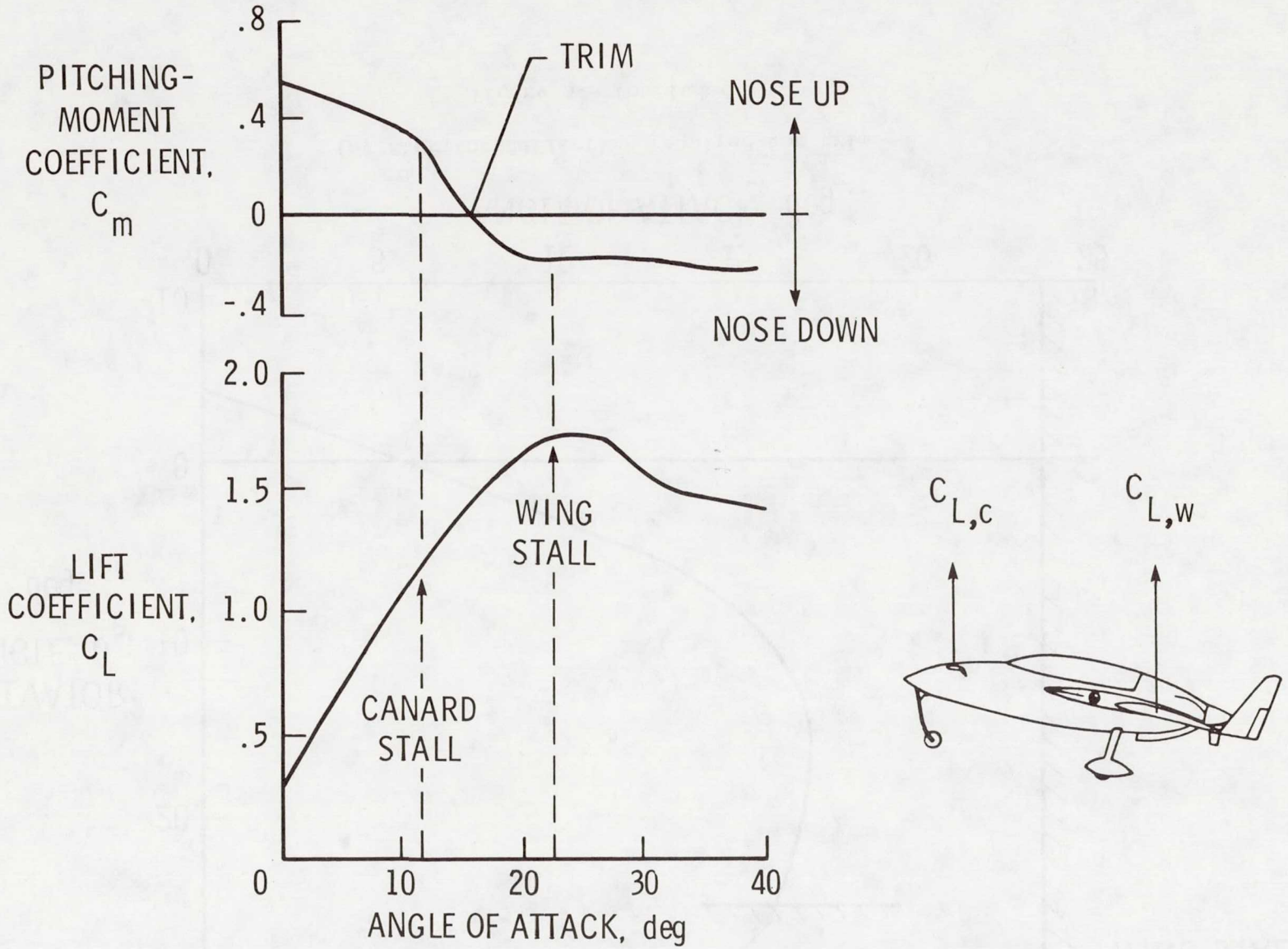

(a) Lift and pitching moment for full nose-up elevator input.

Figure 4.- Longitudinal wind-tunnel data for pusher canard airplane showing stall resistance (ref. 1).

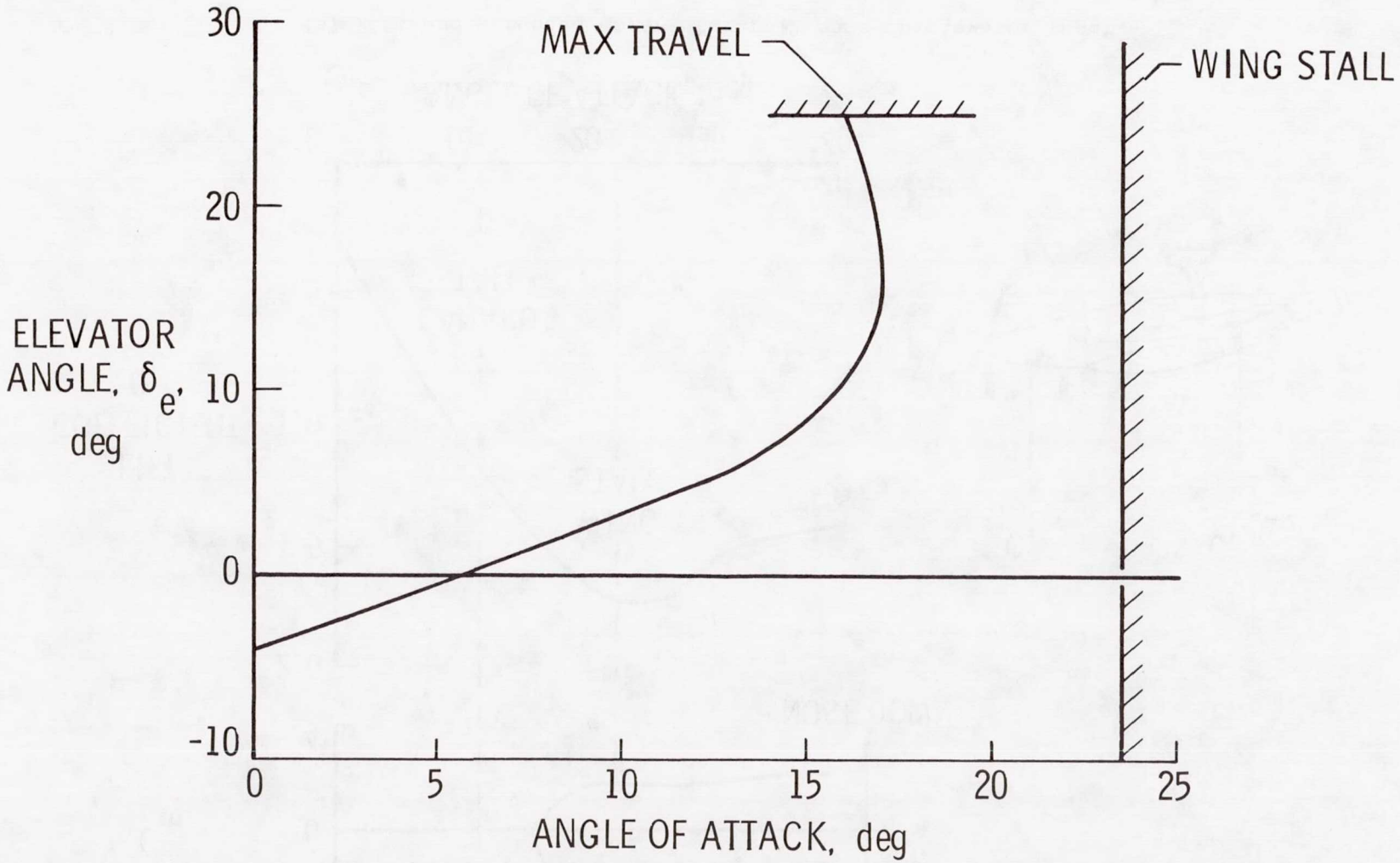

(b) Elevator deflection required for trim.

Figure 4.- Concluded.

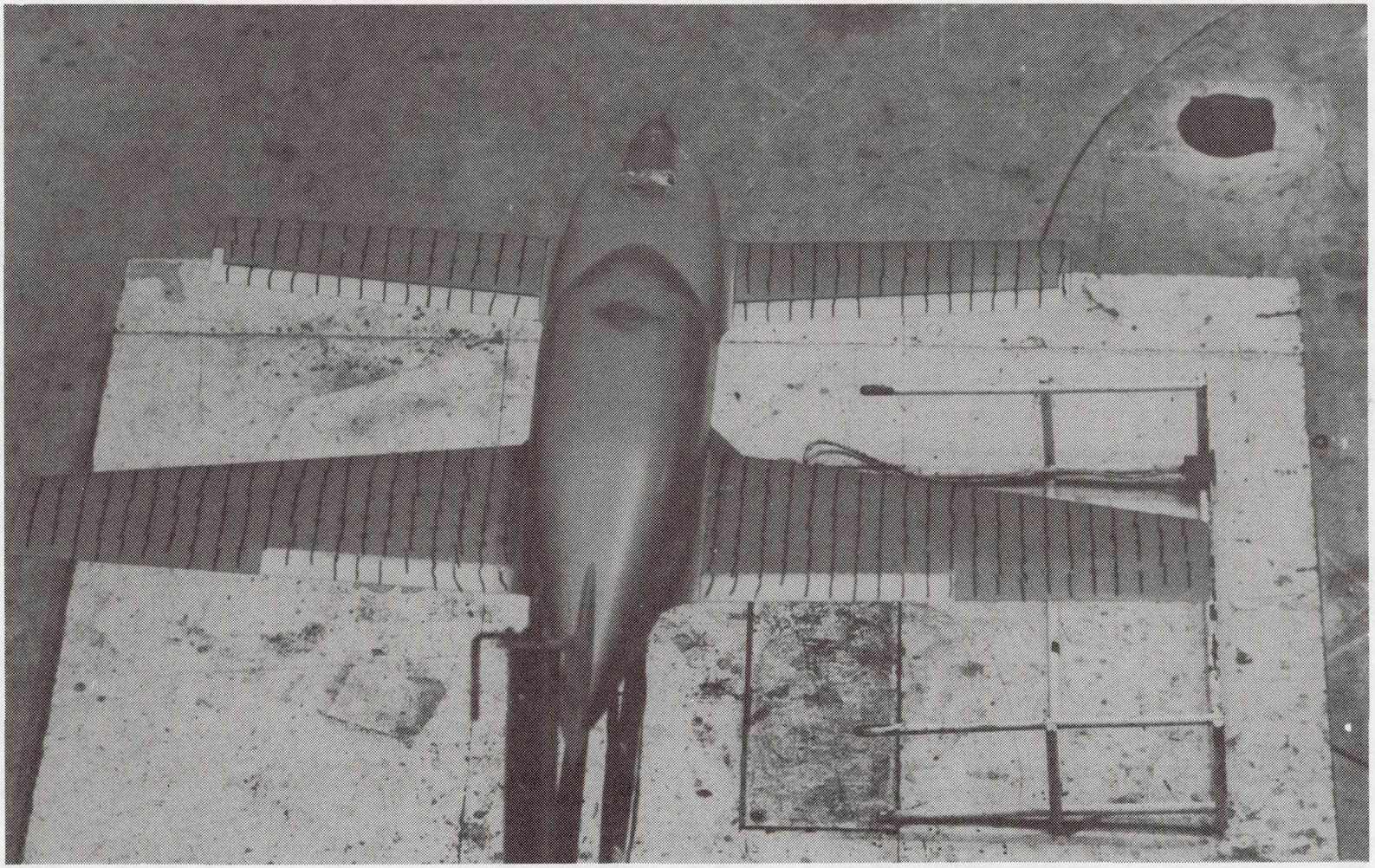

L-84-19

(a) $\alpha = 0°$.

Figure 5.- Flow-visualization results for neutral controls with propeller windmilling.

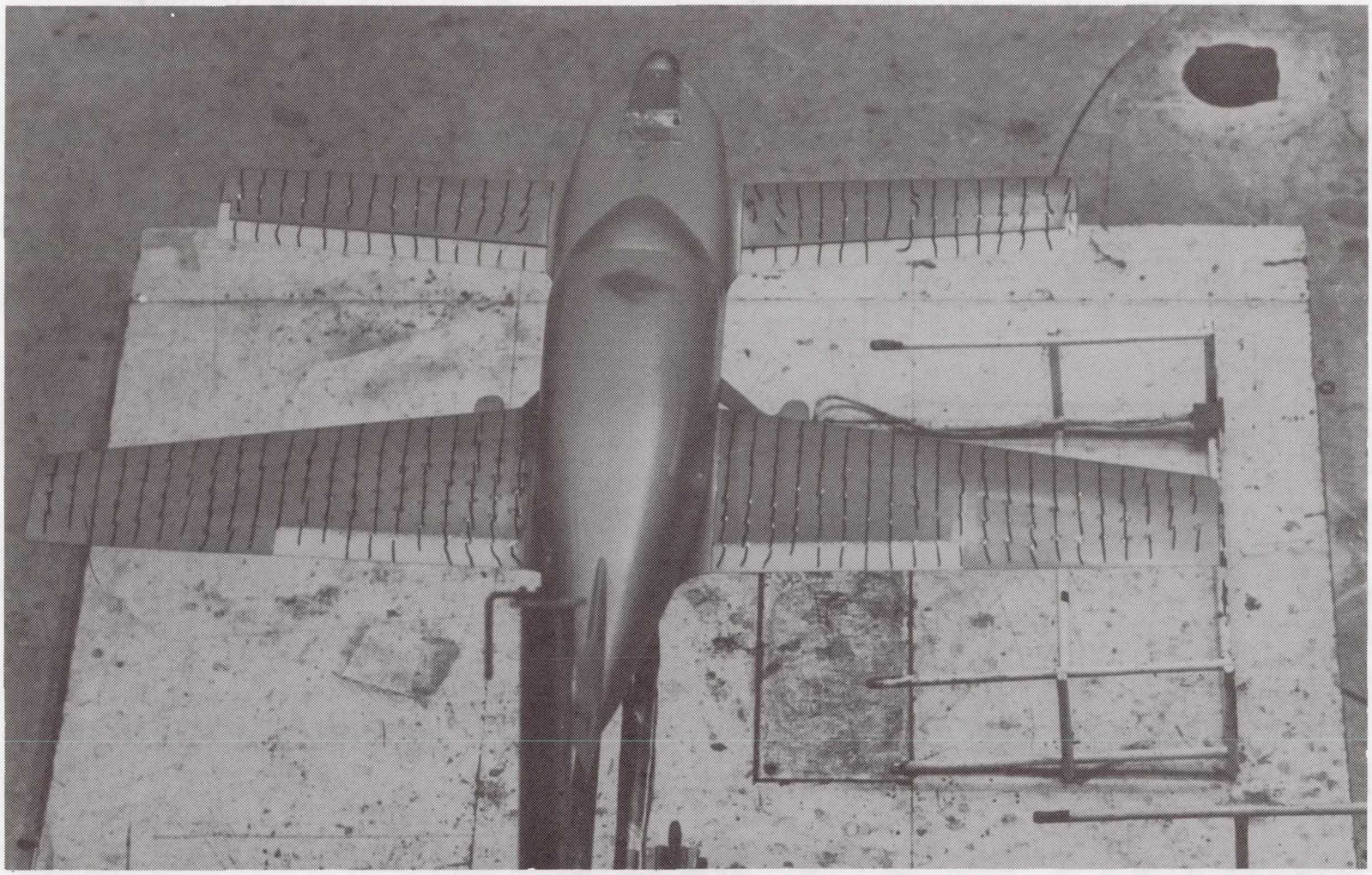

L-84-20

(b) $\alpha = 6°$.

Figure 5.- Continued.

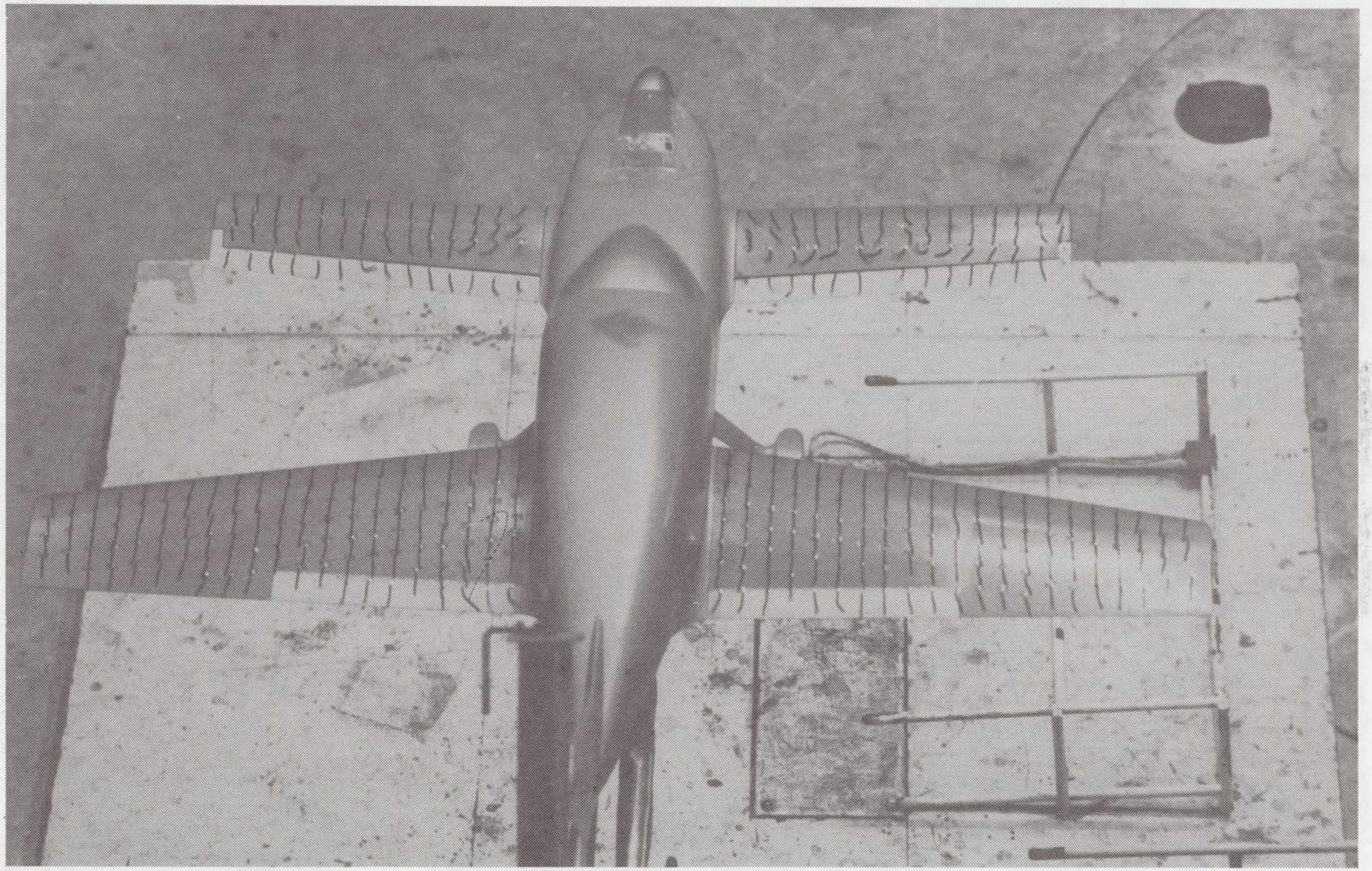

L-84-21

(c) $\alpha = 10°$.

Figure 5.- Continued.

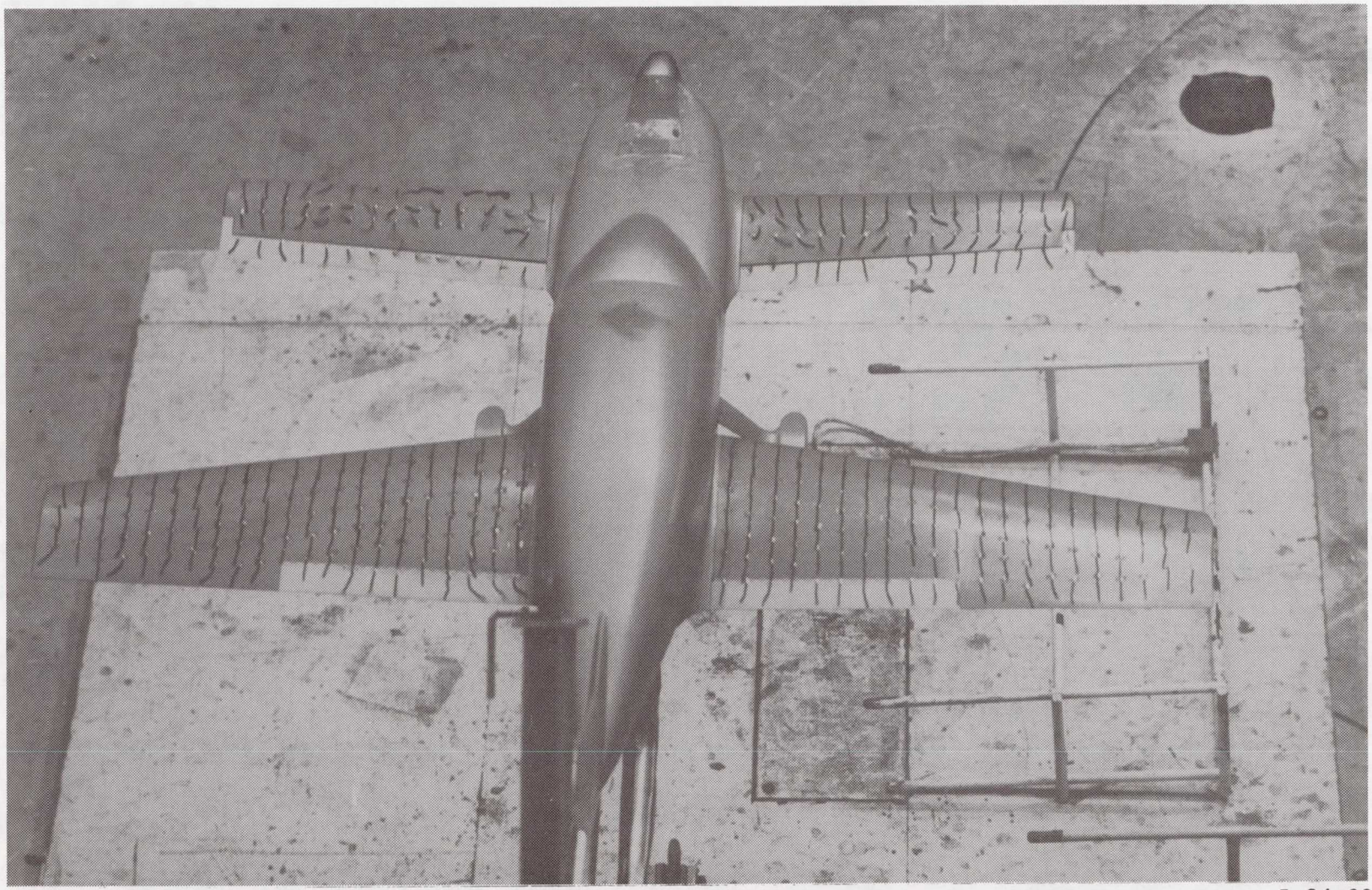

L-84-22

(d) $\alpha = 12°$.

Figure 5.- Continued.

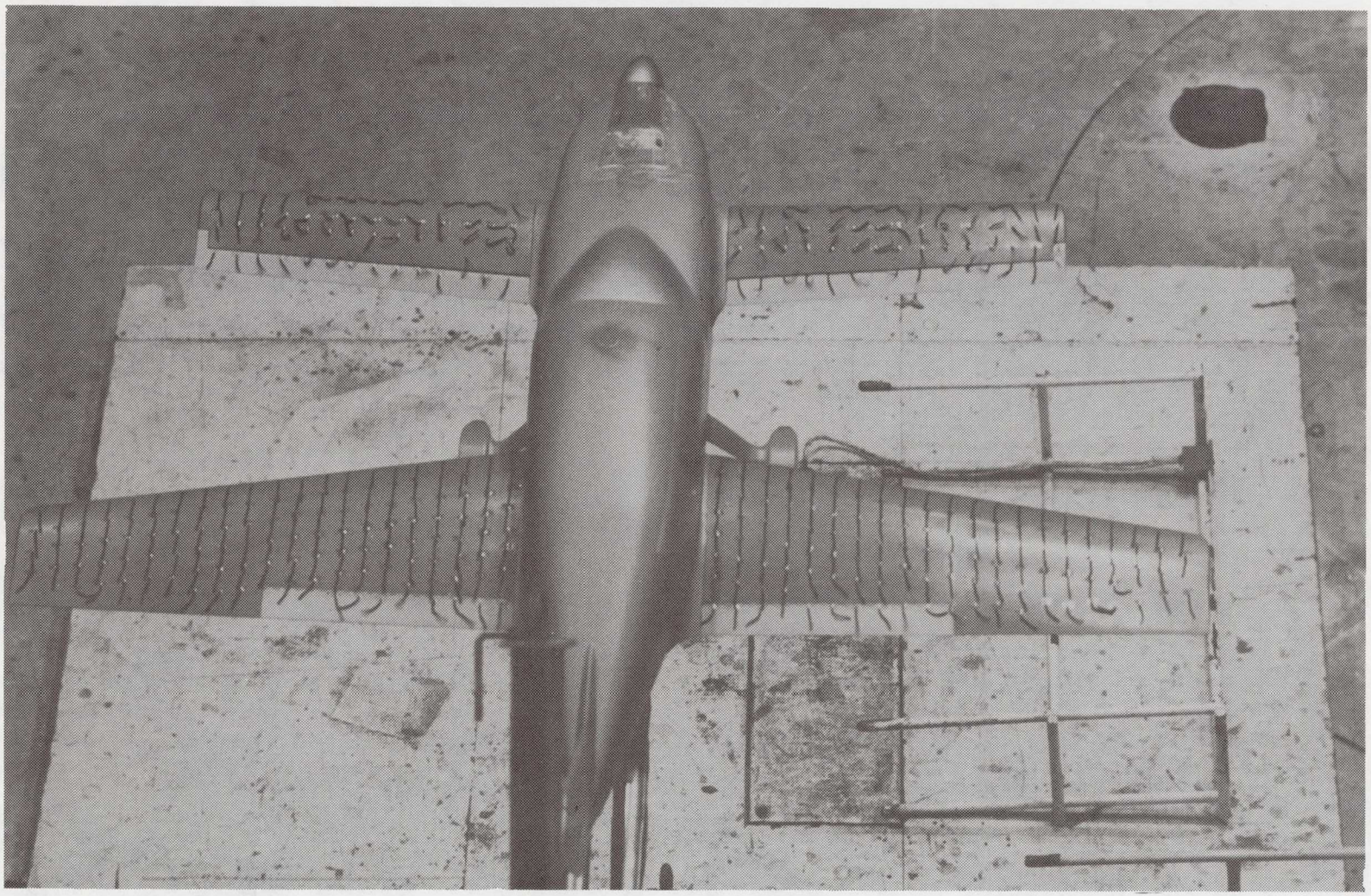

L-84-23

(e) $\alpha = 14°$.

Figure 5.- Continued.

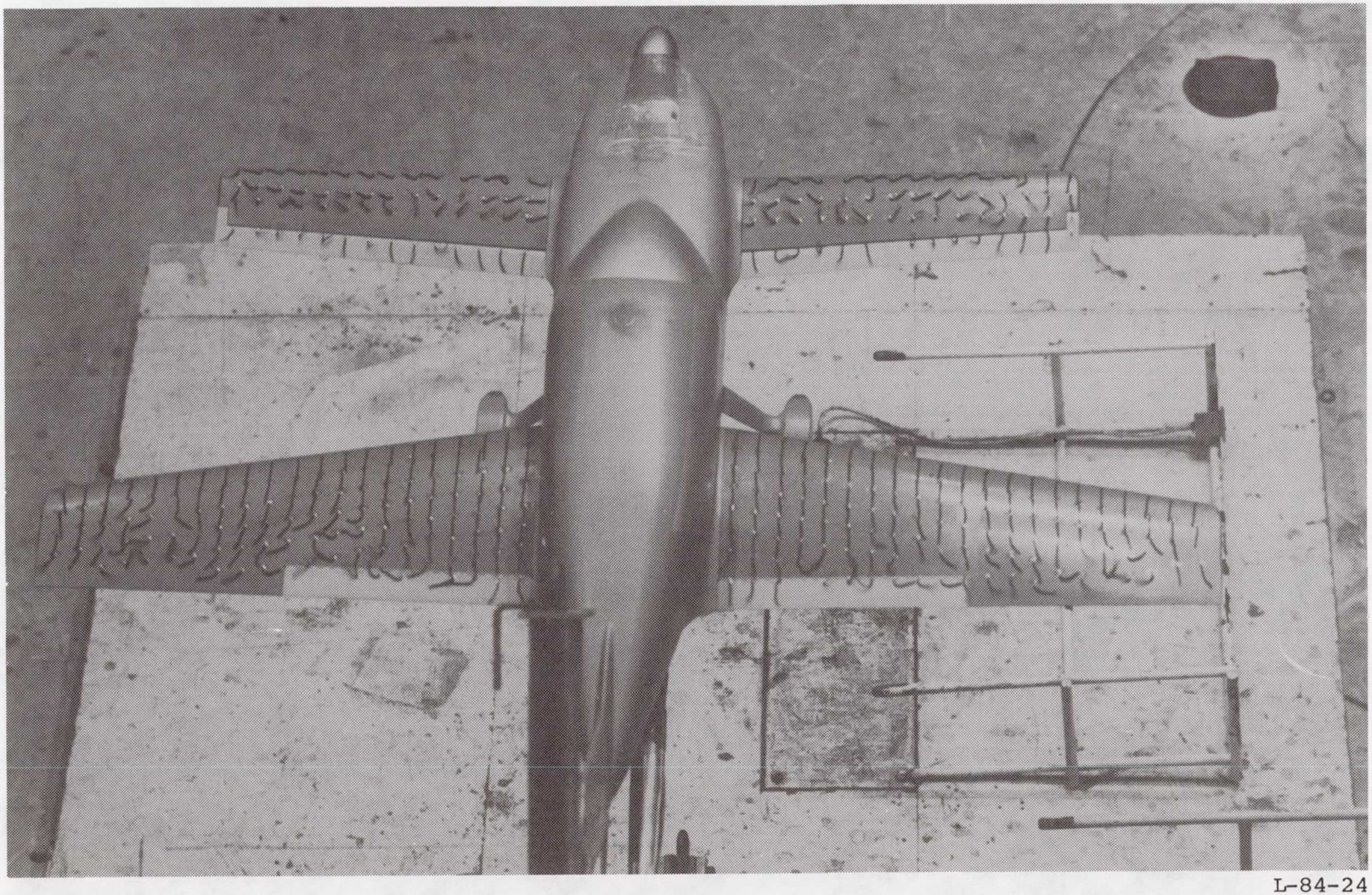

L-84-24

(f) $\alpha = 16°$.

Figure 5.- Continued.

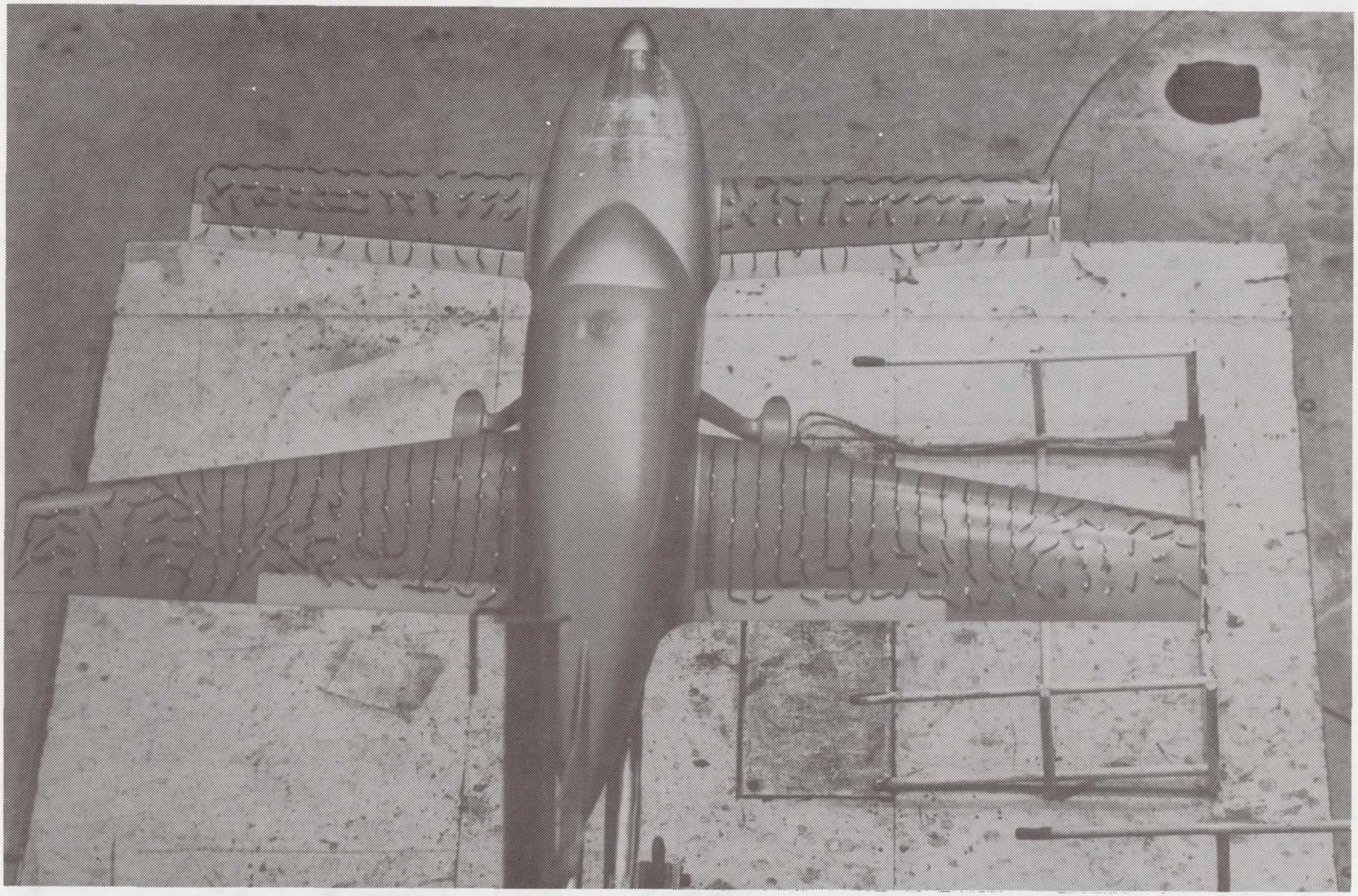

(g) $\alpha = 18°$.

L-84-25

Figure 5.- Continued.

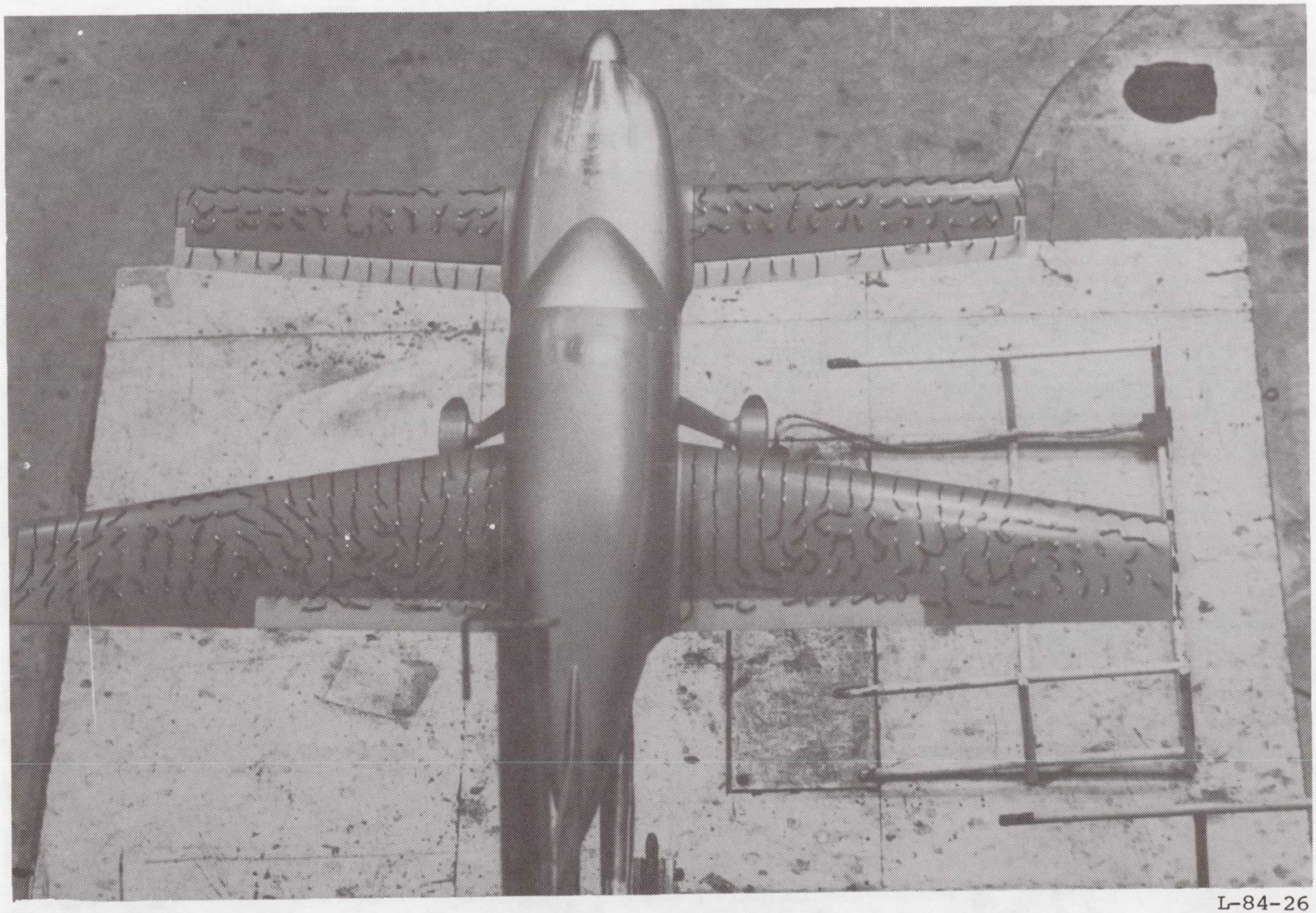

L-84-26

(h) $\alpha = 22°$.

Figure 5.- Concluded.

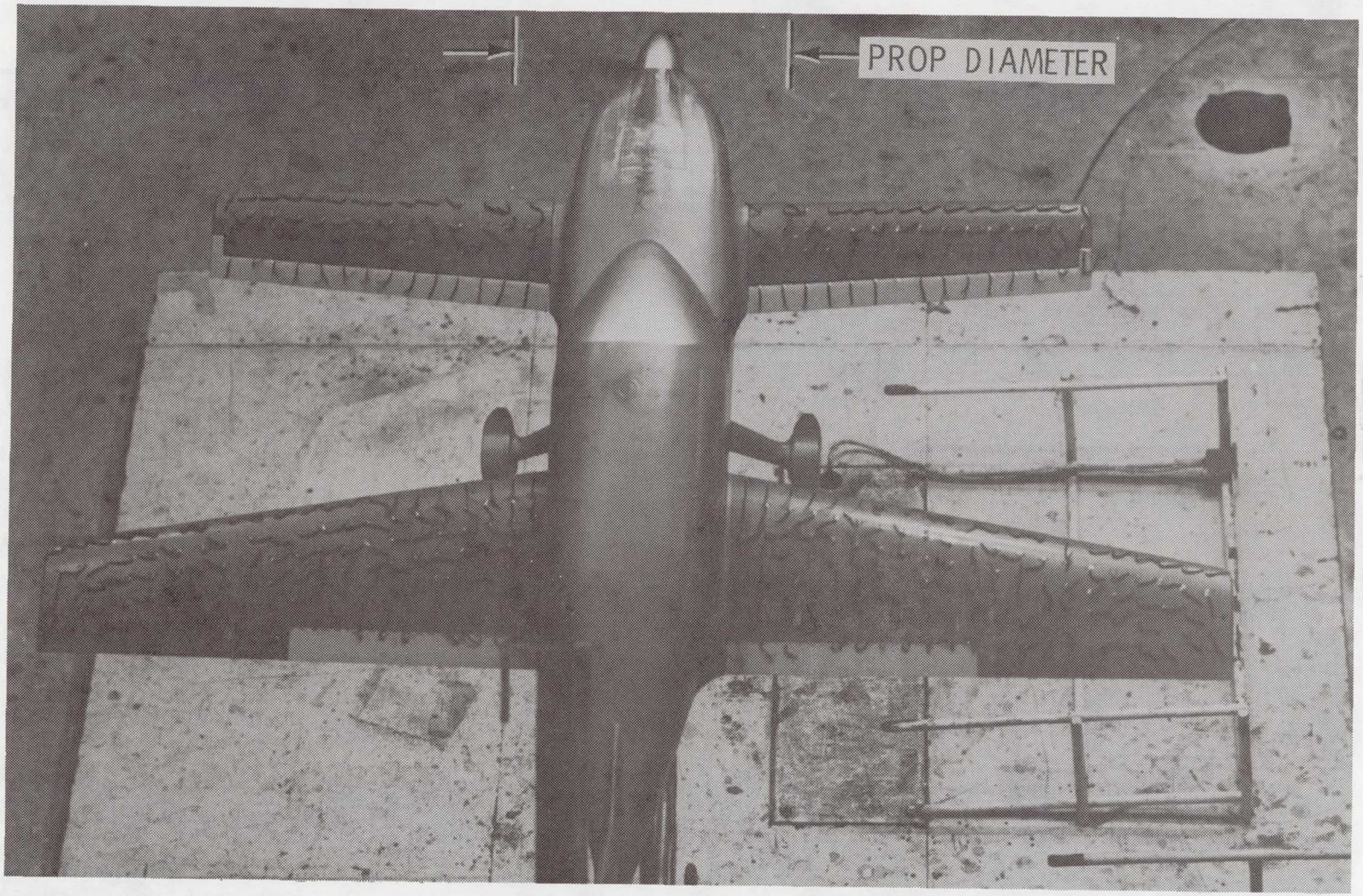

L-84-27

(a) Windmilling propeller.

Figure 6.- Typical effects of power at post-stall angles of attack. $\alpha = 28°$.

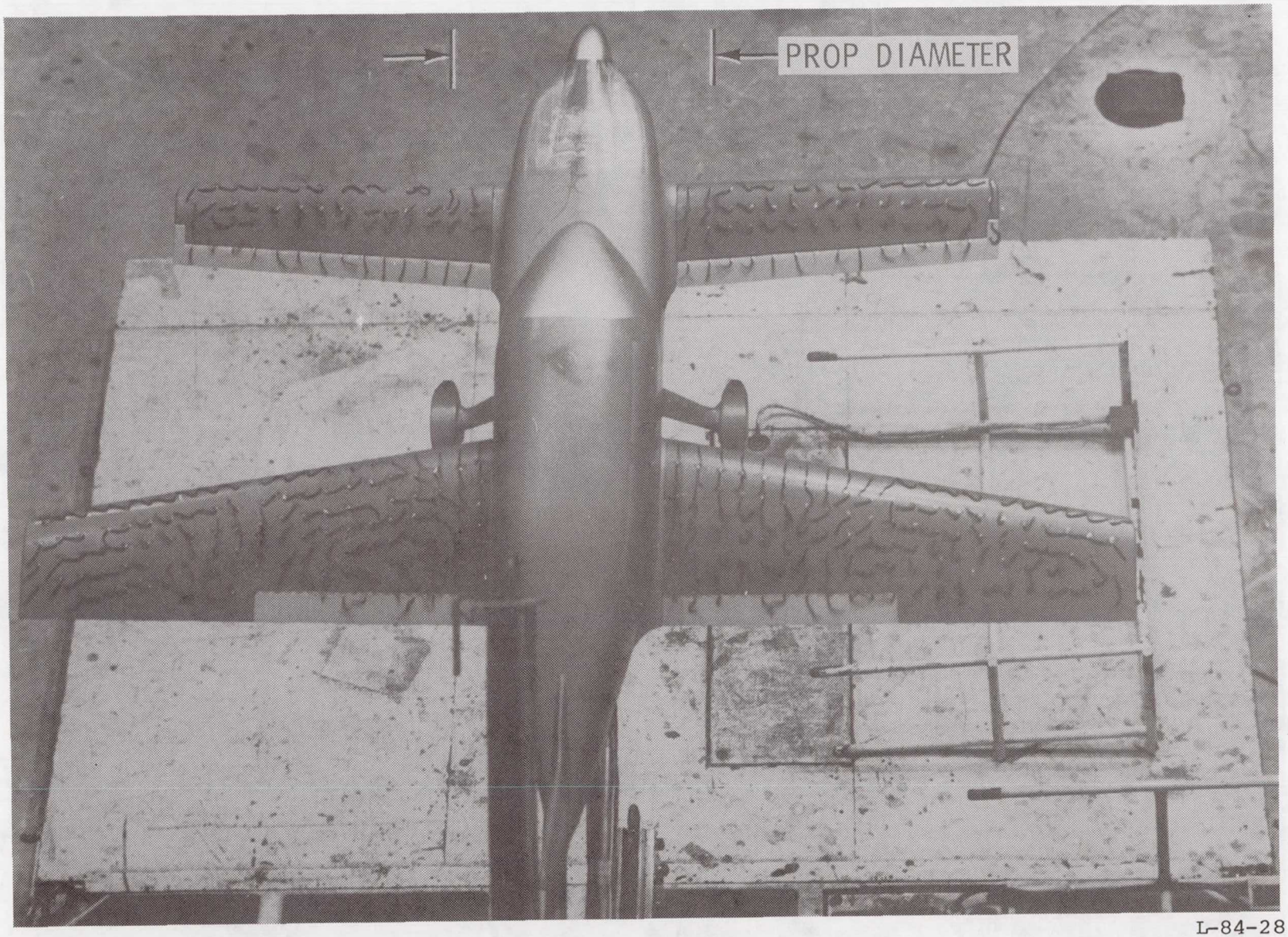

L-84-28

(b) $C_T = 0.4$.

Figure 6.- Concluded.

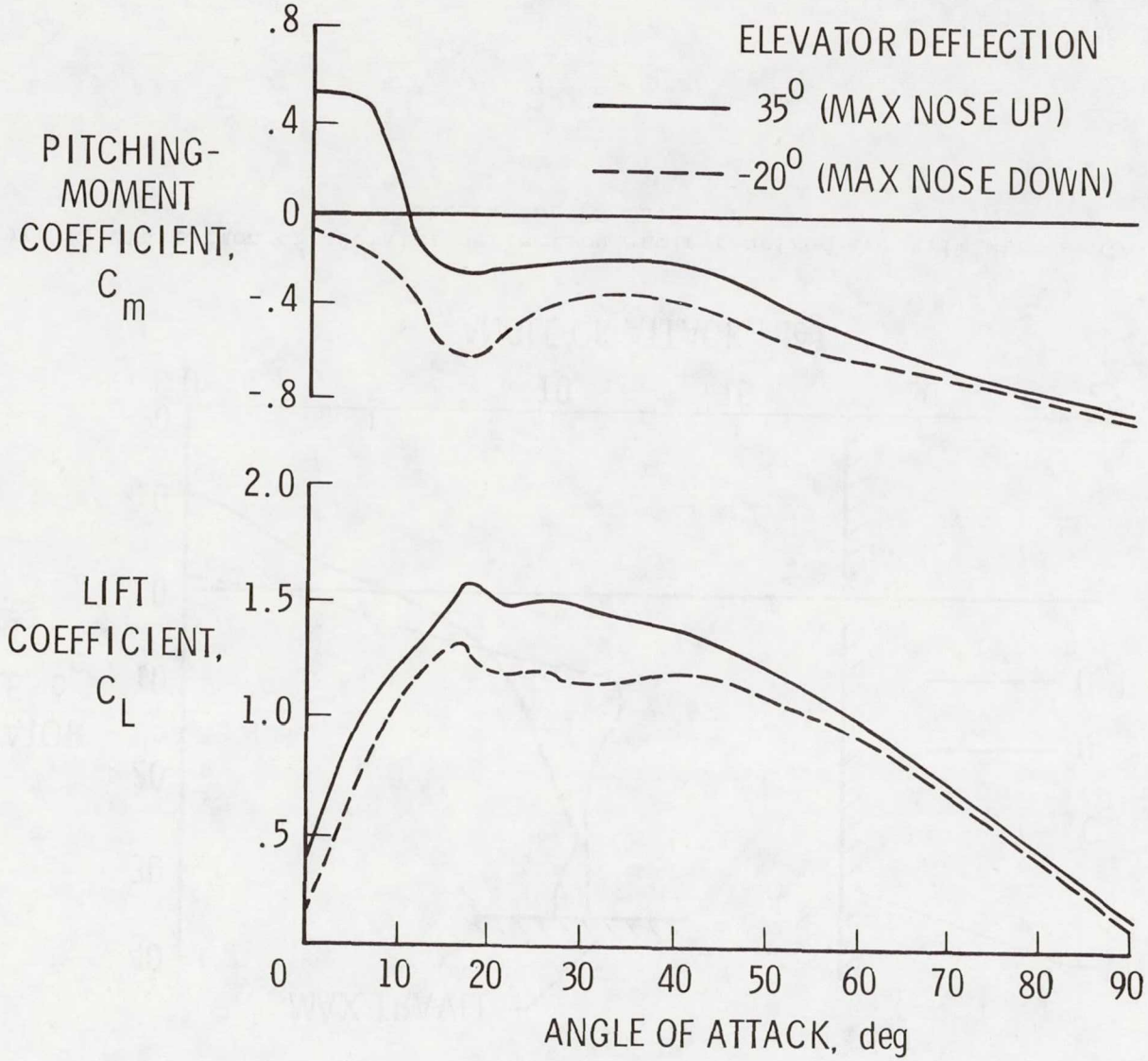

Figure 7.- Longitudinal characteristics for forward center-of-gravity location of FS 23.3 in. with power off.

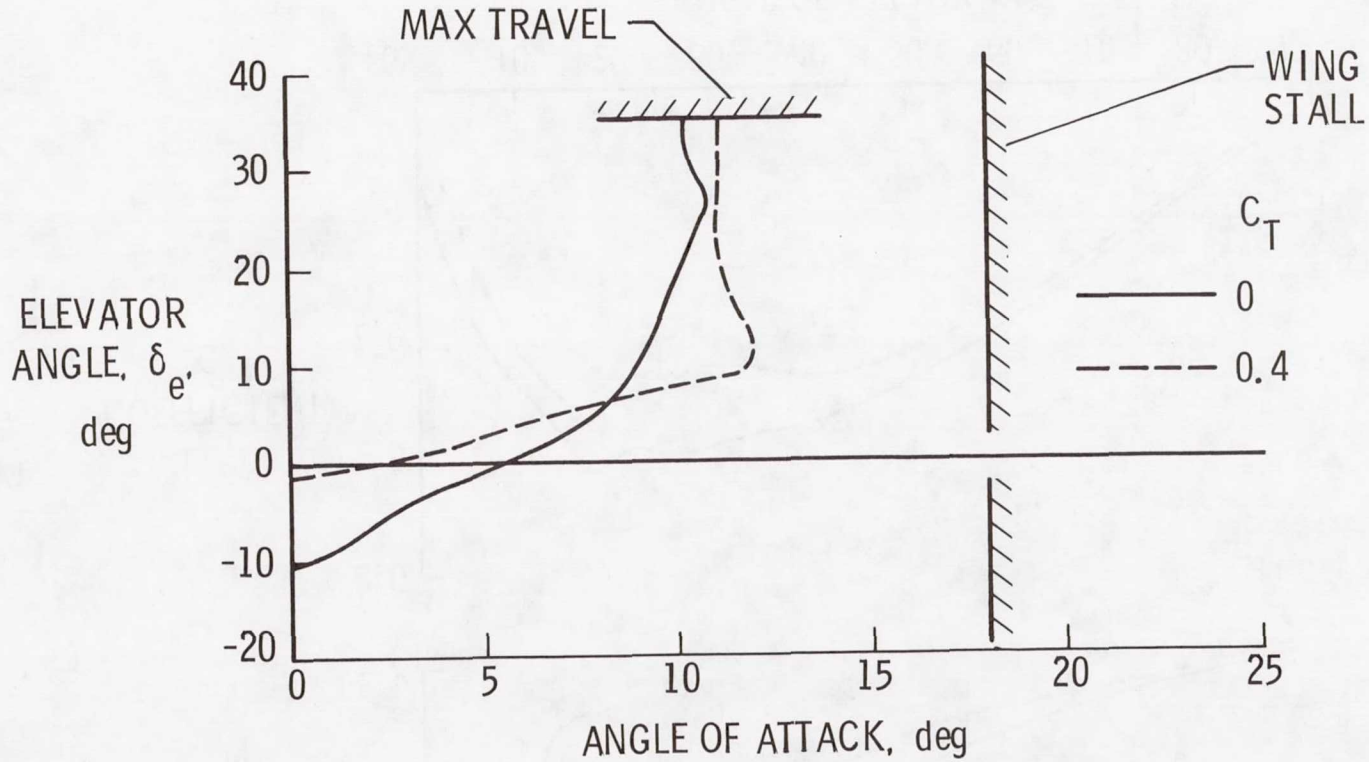

Figure 8.- Variation of elevator deflection angle required for trim with angle of attack for FS 23.3 in.

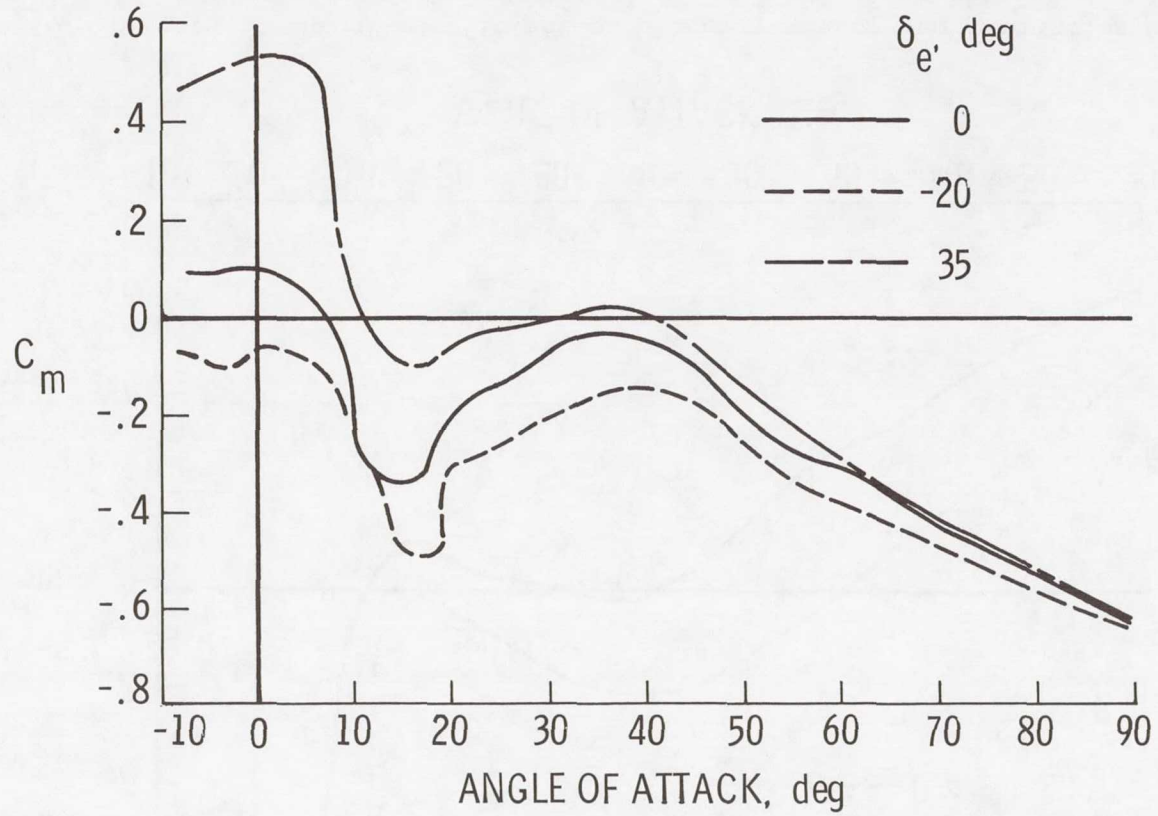

Figure 9.- Aerodynamic pitching moments for aft center-of-gravity location of FS 24.8 in. with power off.

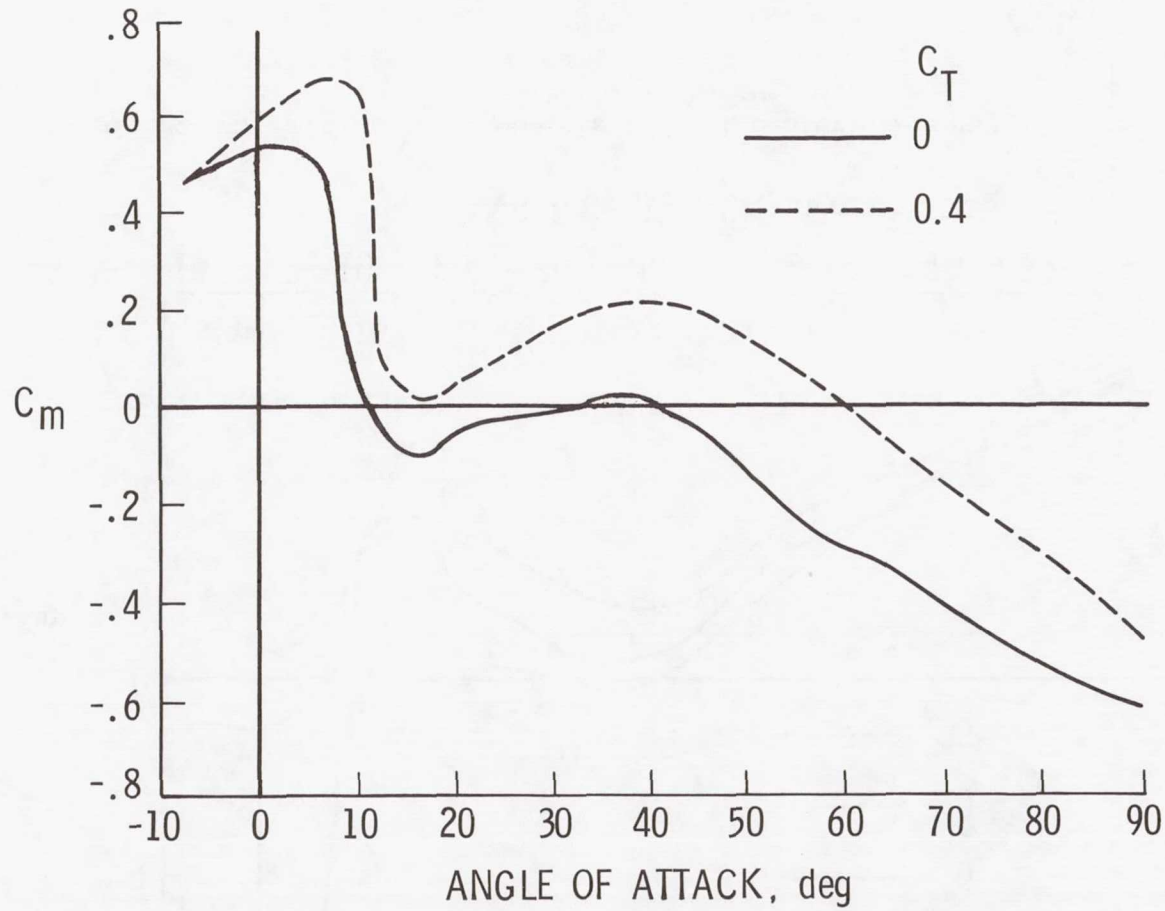

Figure 10.- Effects of thrust coefficient on pitching-moment characteristics for aft center-of-gravity location of FS 24.8 in. $\delta_e = 35°$.

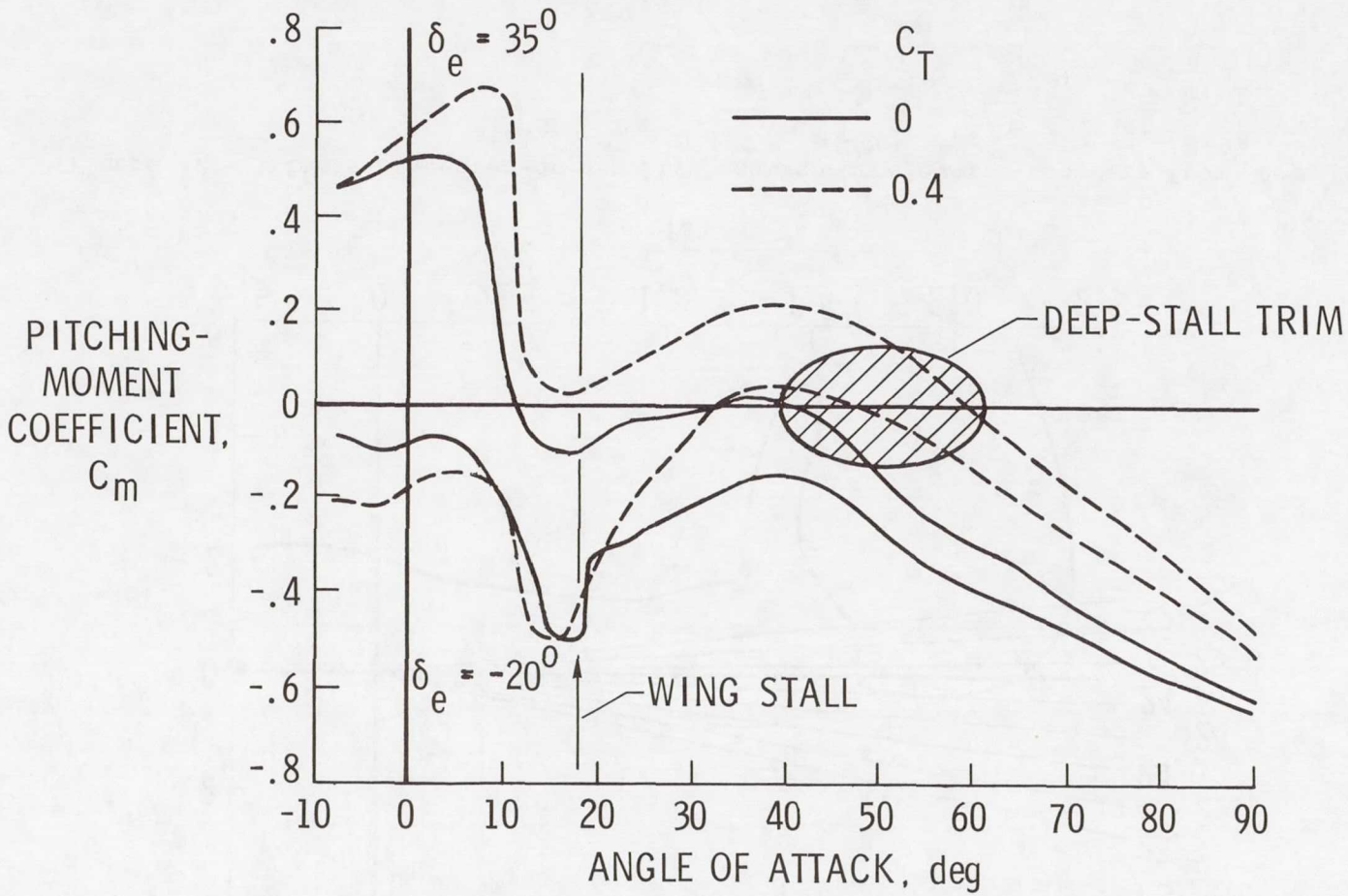

Figure 11.- Effect of elevator deflection on deep stall trim condition.
Center of gravity at FS 24.8 in.

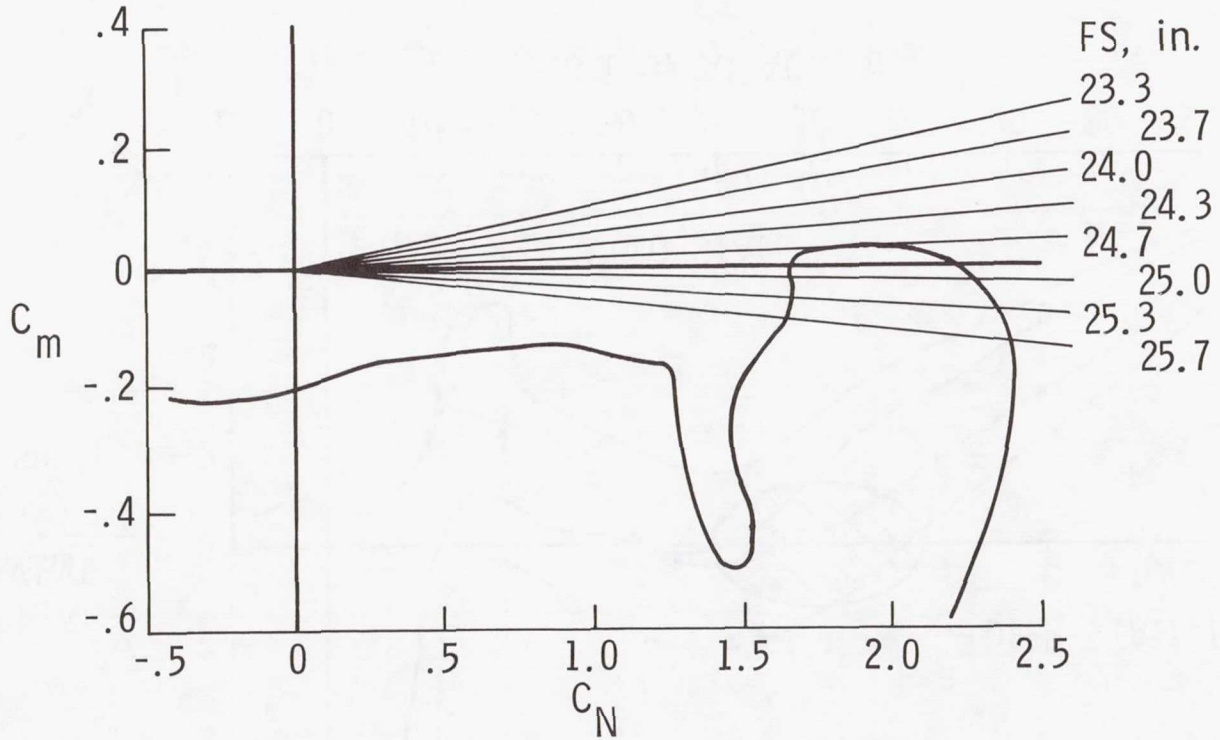

Figure 12.- Effects of center-of-gravity location on elevator recovery from deep stall. $C_T = 0.4$; $\delta_e = -20°$.

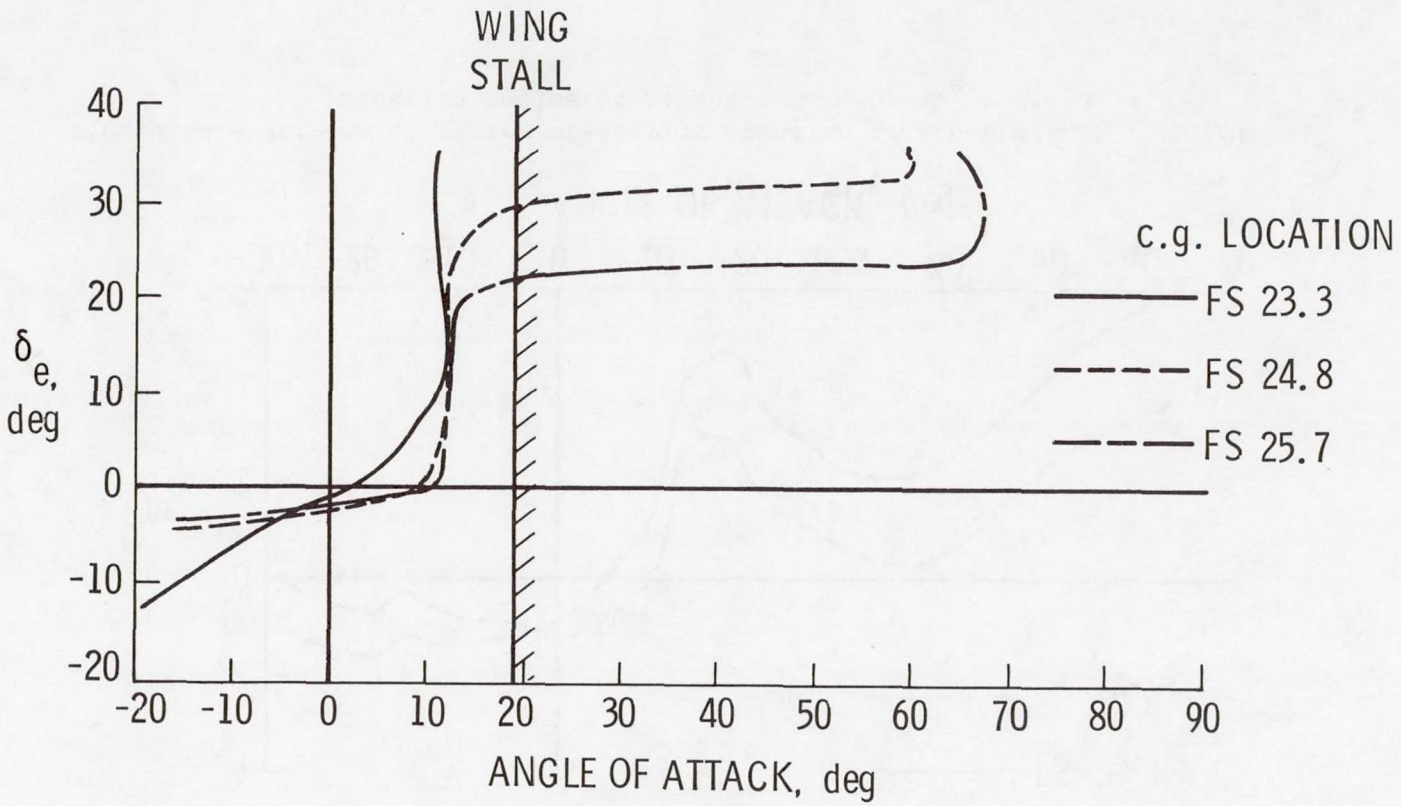

Figure 13.- Effects of center-of-gravity location on elevator deflection angle required for trim. $C_T = 0.4$.

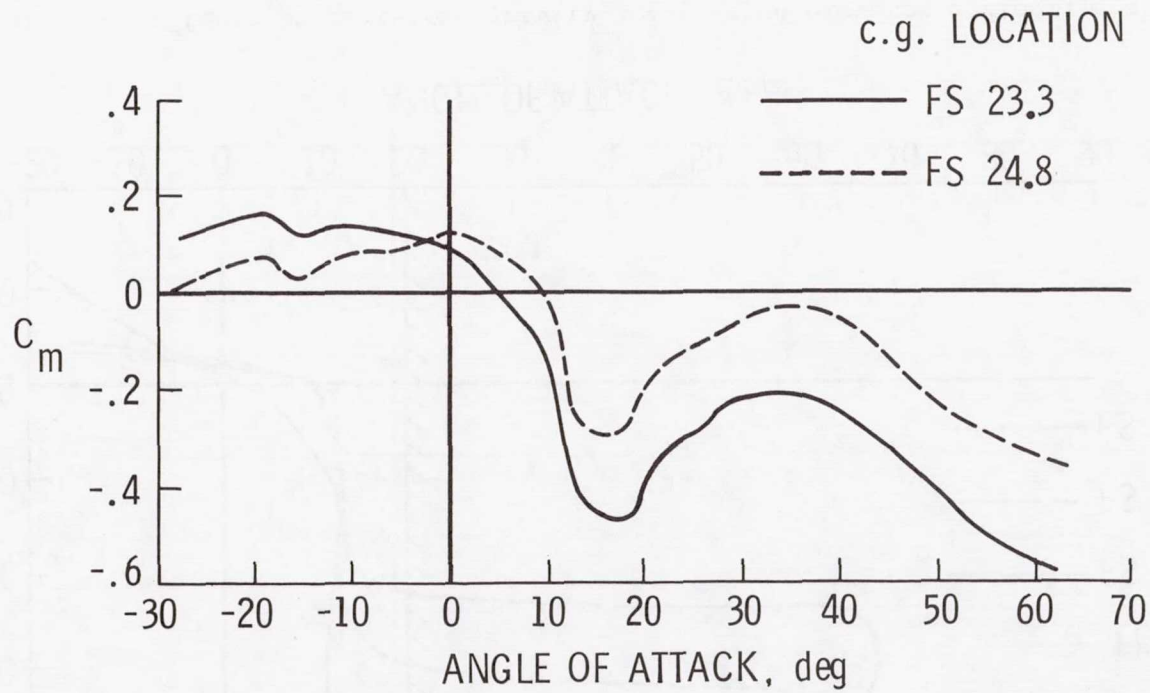

Figure 14.- Effects of center-of-gravity location on longitudinal stability at negative angles of attack. $C_T = 0$; $\delta_e = 0°$.

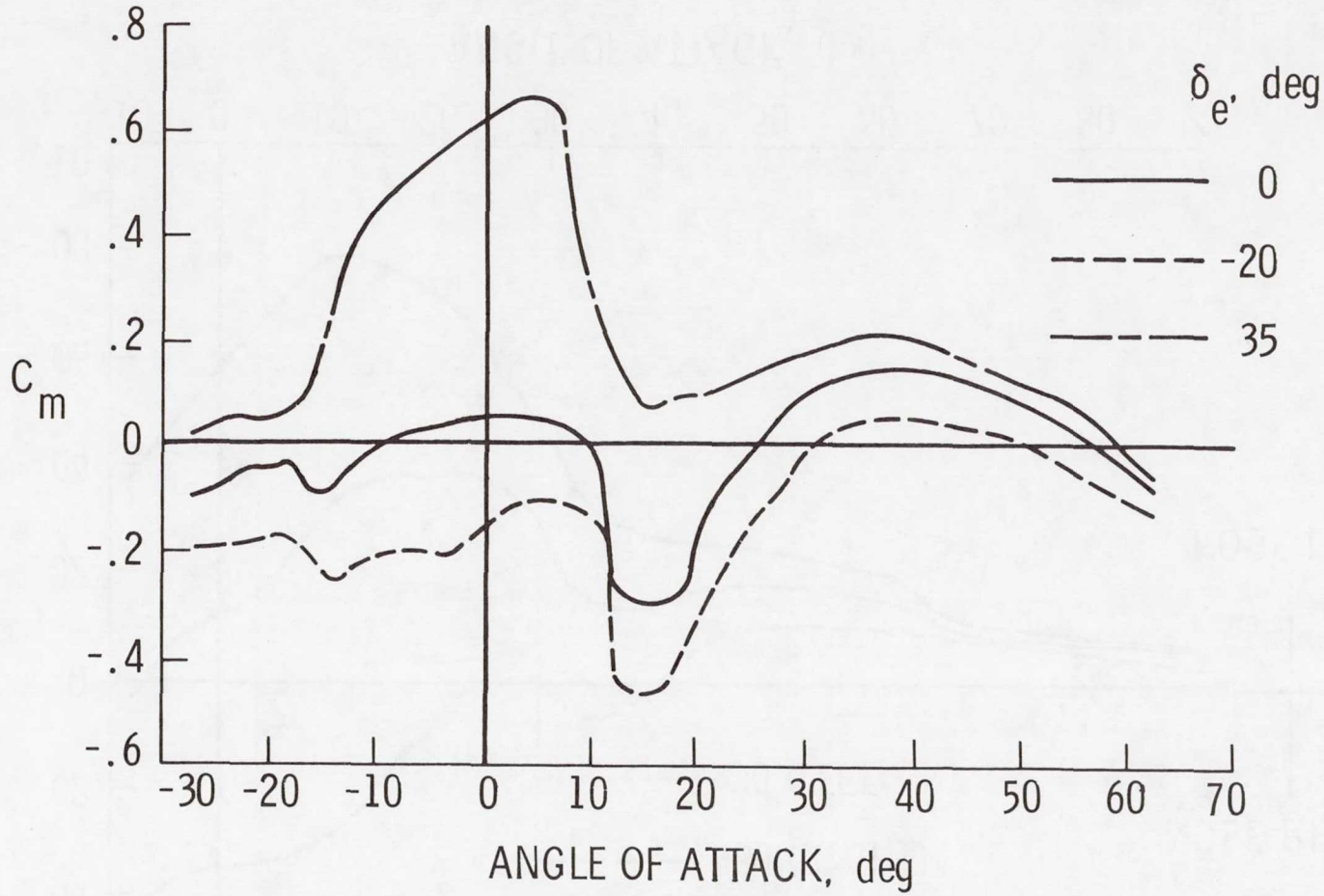

Figure 15.- Elevator effectiveness at negative angles of attack for center of gravity at FS 24.8 in. $C_T = 0.4$.

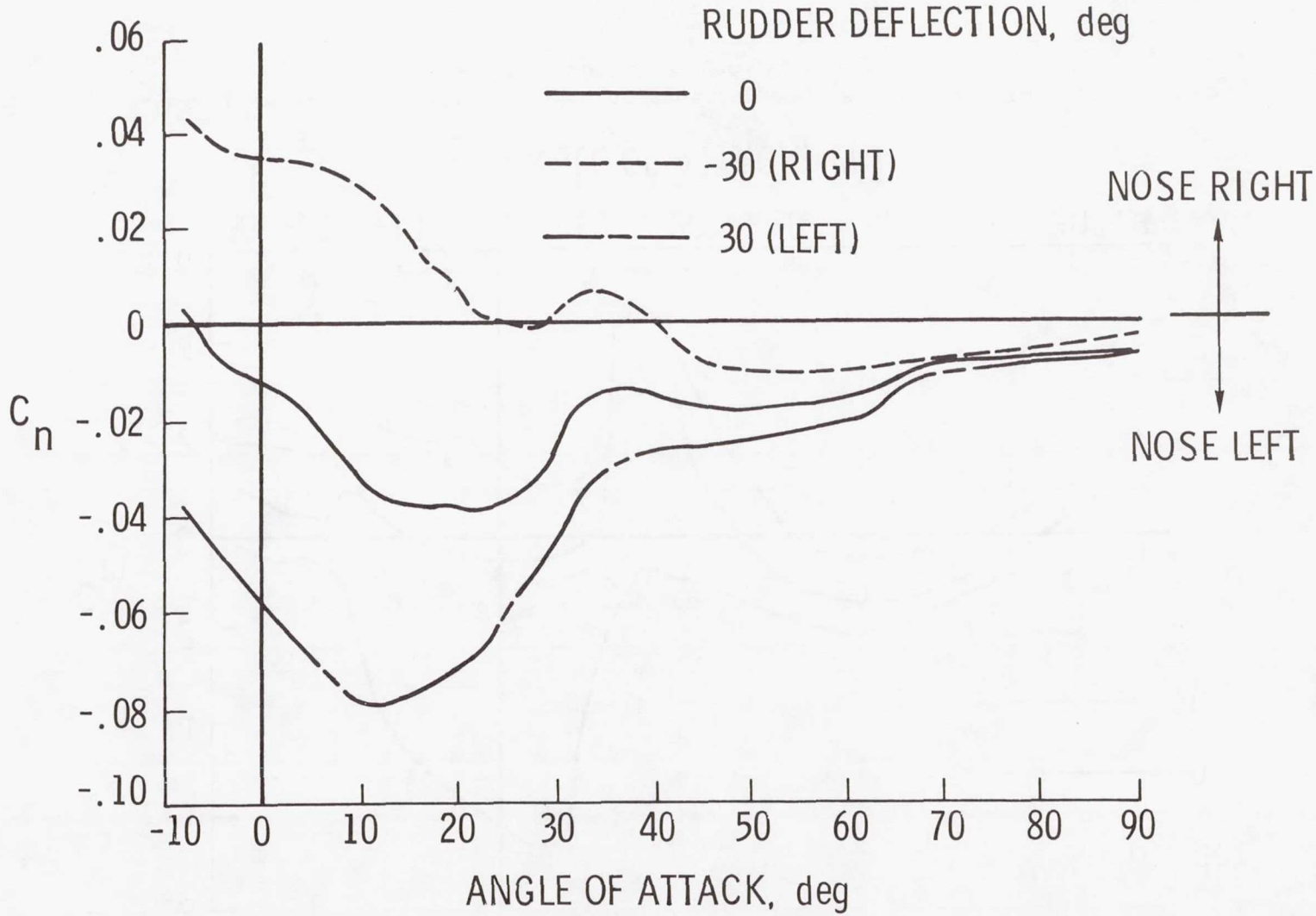

Figure 16.- Variations of yawing-moment coefficient with angle of attack and rudder deflection. $C_T = 0.4$.

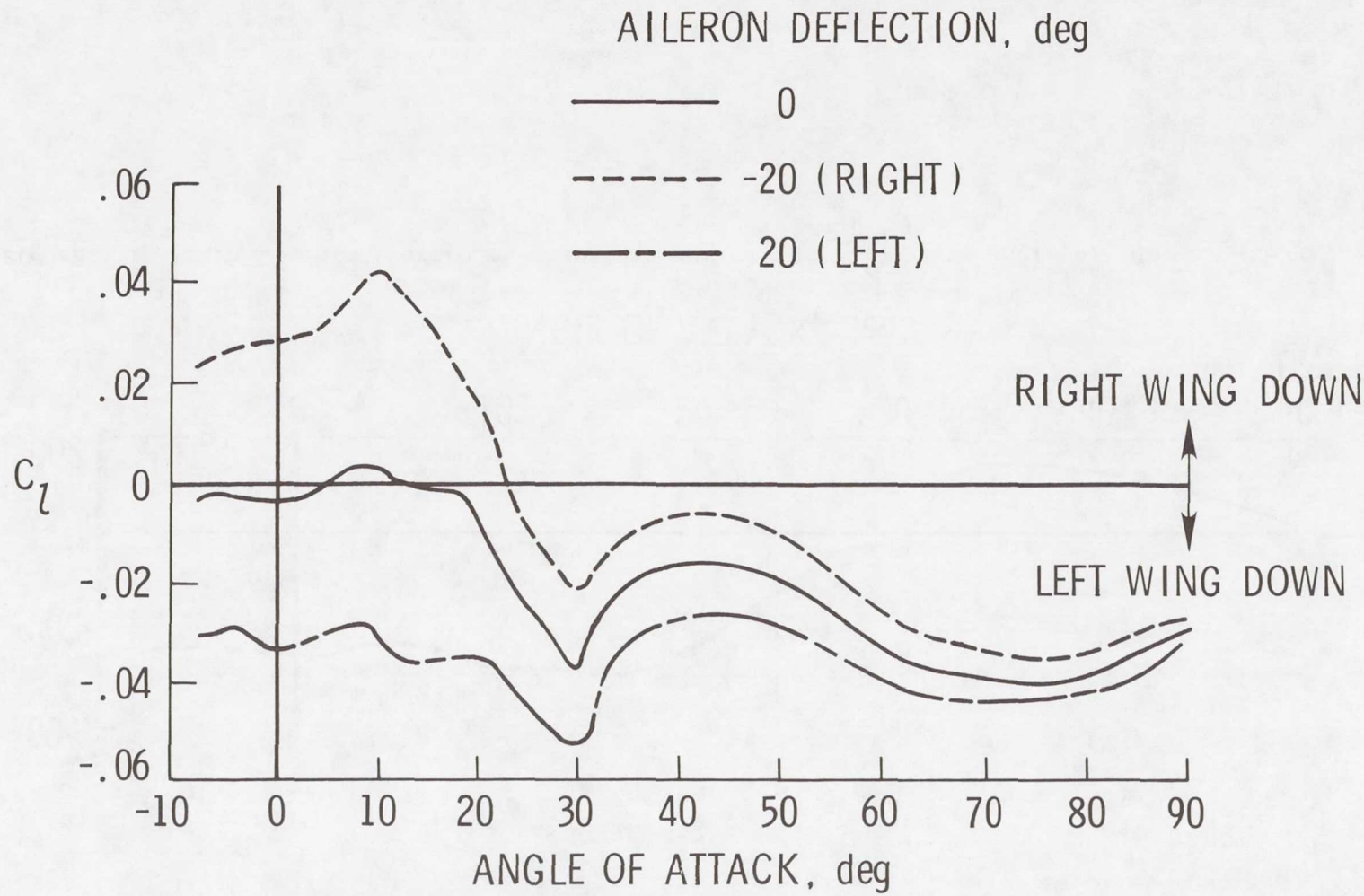

Figure 17.- Variation of rolling-moment coefficient C_l with angle of attack and aileron deflection. $C_T = 0.4$.

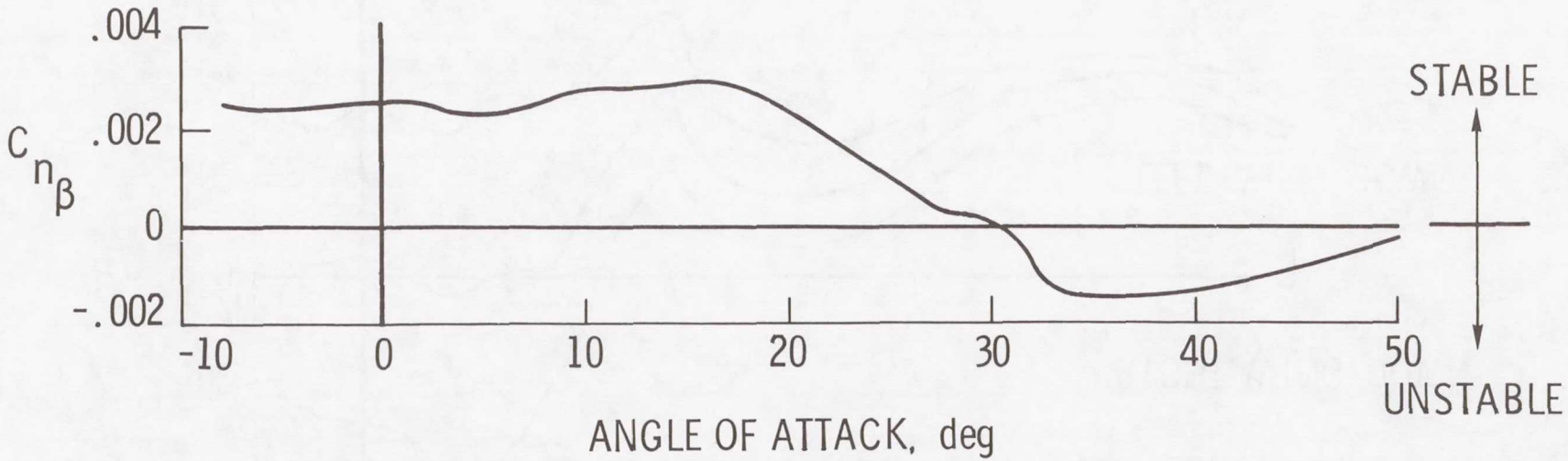

Figure 18.- Variation of directional-stability derivative C_{n_β} with angle of attack. $C_T = 0.4$.

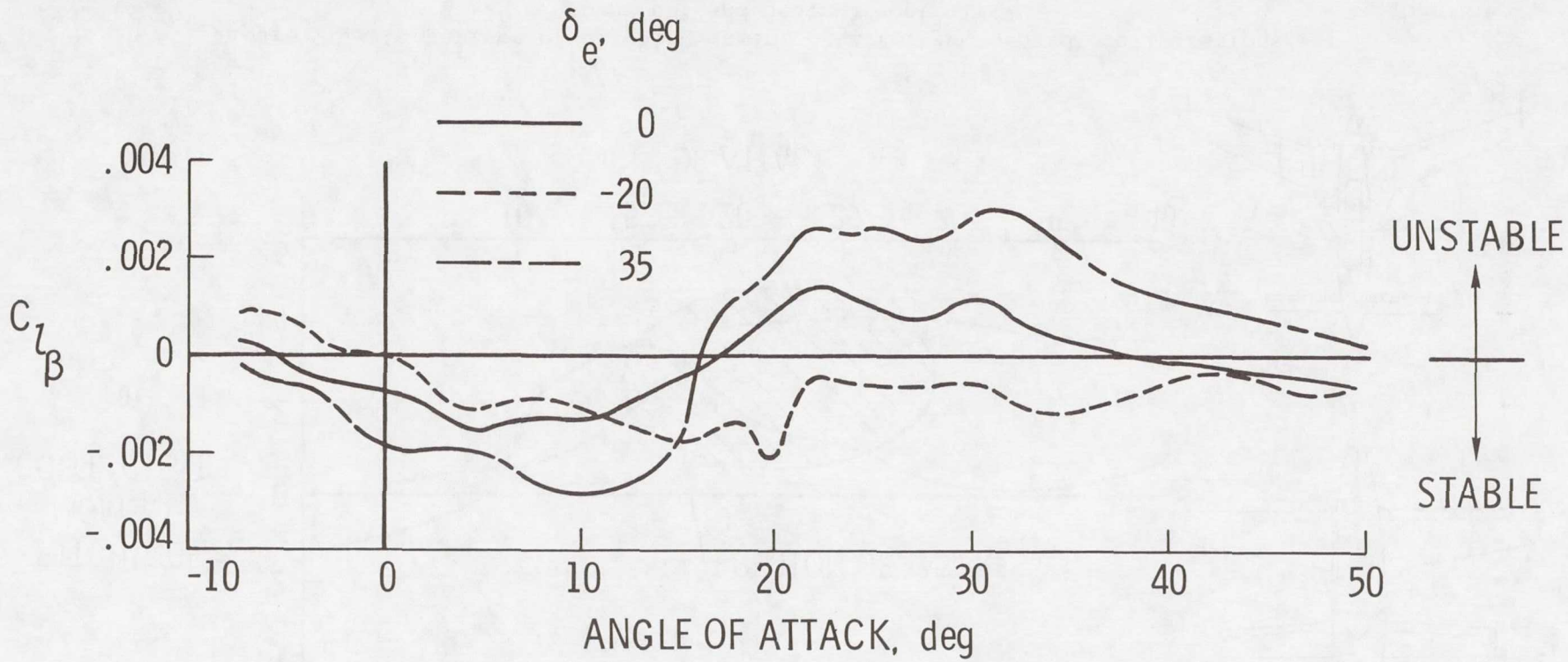

Figure 19.- Effects of elevator deflection angle on dihedral effect. $C_T = 0.4$.

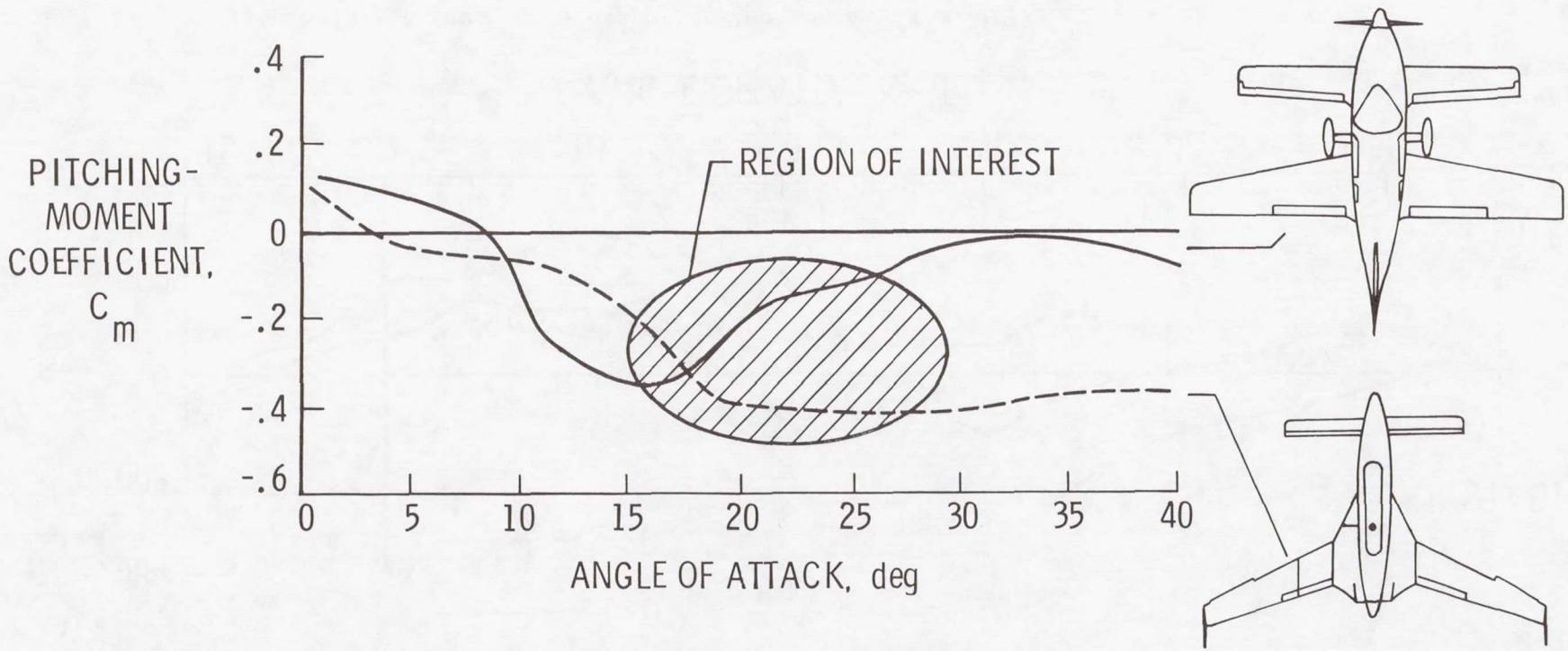

Figure 20.- Comparison of pitching-moment data for two canard configurations for power off and neutral controls.

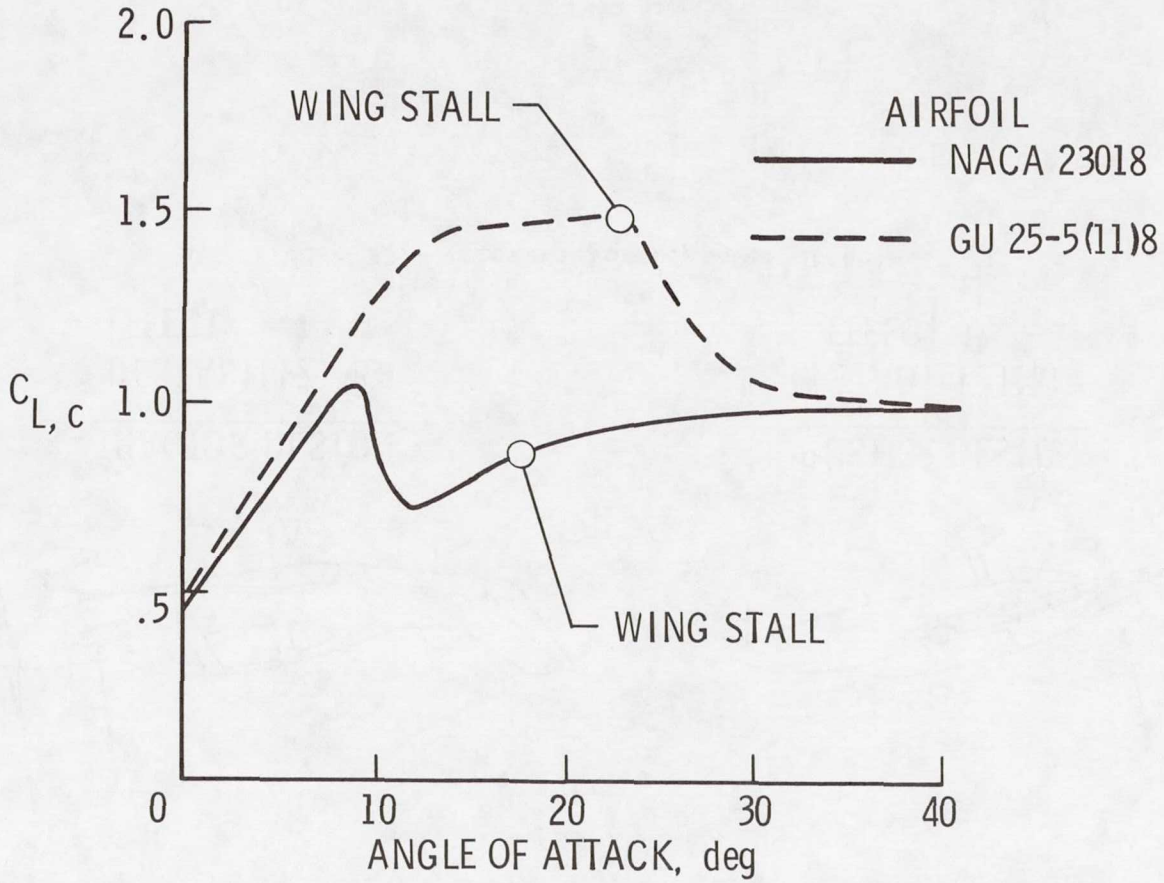

Figure 21.- Comparison of canard lift characteristics.

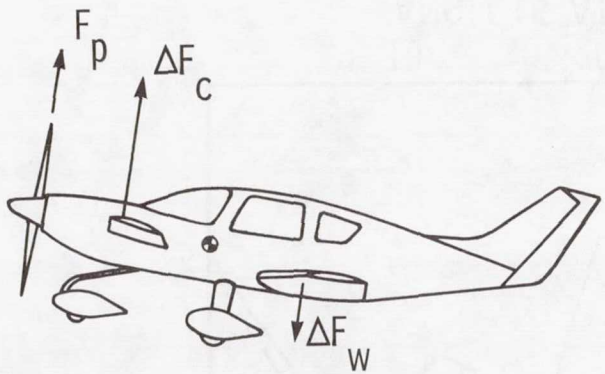

TRACTOR DESIGN

- DESTABILIZING EFFECT

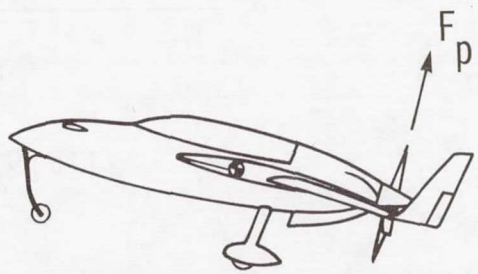

PUSHER DESIGN

- STABILIZING EFFECT

Figure 22.- Illustration of power effects.

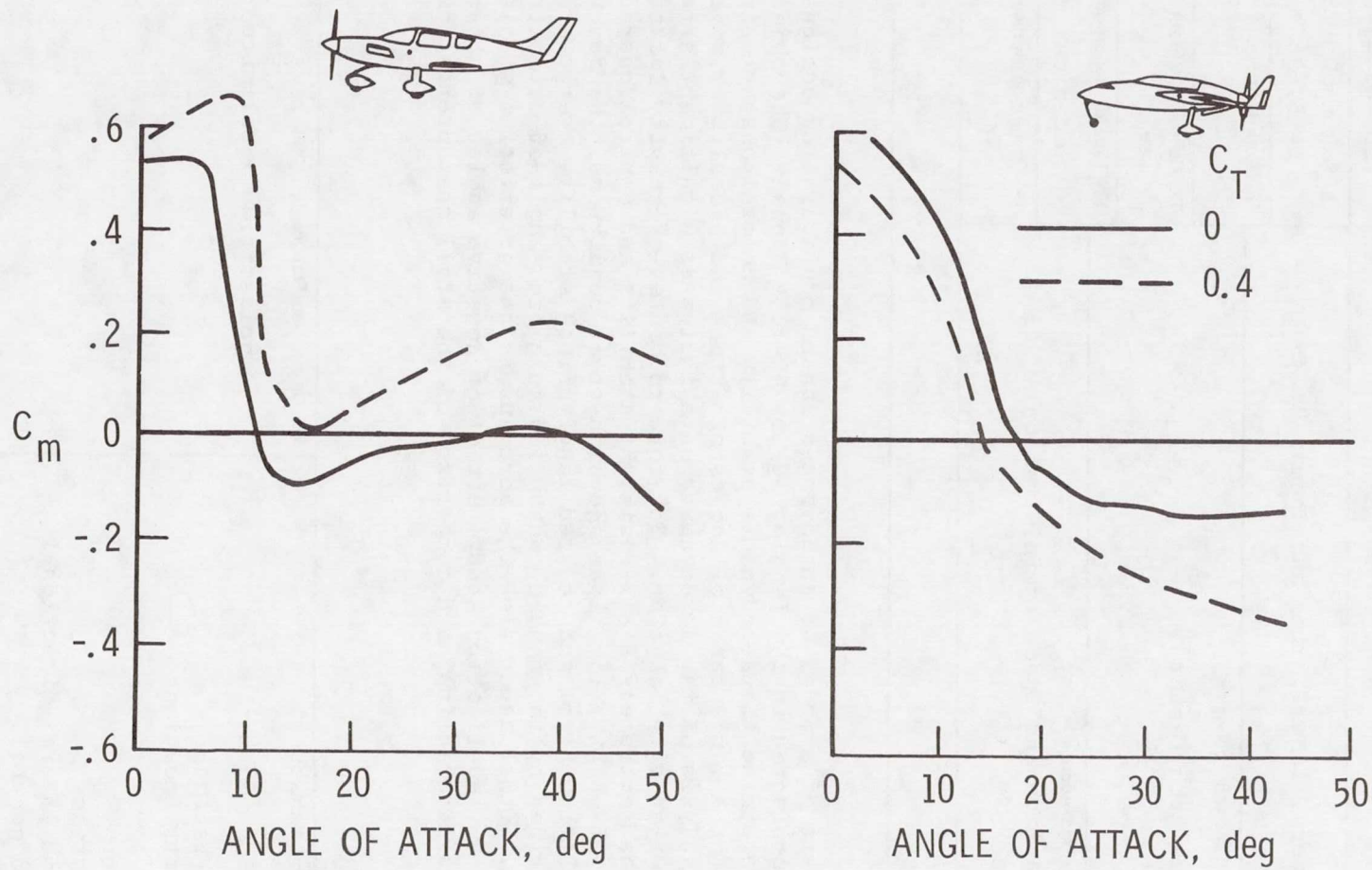

Figure 23.- Effect of power on pitching-moment coefficient.

1. Report No.	2. Government Accession No.	3. Recipient's Catalog No.
NASA TM-85760		

4. Title and Subtitle	5. Report Date
WIND-TUNNEL INVESTIGATION OF AN ADVANCED GENERAL AVIATION CANARD CONFIGURATION	April 1984
	6. Performing Organization Code 505-45-43-01
7. Author(s) Joseph R. Chambers, Long P. Yip, and Thomas M. Moul	8. Performing Organization Report No. L-15713
	10. Work Unit No.
9. Performing Organization Name and Address NASA Langley Research Center Hampton, VA 23665	11. Contract or Grant No.
	13. Type of Report and Period Covered Technical Memorandum
12. Sponsoring Agency Name and Address National Aeronautics and Space Administration Washington, DC 20546	14. Sponsoring Agency Code

15. Supplementary Notes

16. Abstract

Wind-tunnel tests of a model of an advanced canard configuration designed for general aviation were conducted in the Langley 30- by 60-Foot Tunnel. The objective of the tests was to determine the aerodynamic stability and control characteristics of the configuration for a large range of angles of attack and sideslip at several power conditions. Analysis of the aerodynamic data indicates significant effects of power and of center-of-gravity location. For forward center-of-gravity locations, the configuration had extremely stall-resistant stability and control characteristics. For aft center-of-gravity locations and high-power conditions, the combined effects of increased pitch control and reduced longitudinal stability overpowered the stall resistance provided by the canard, which led to a high-angle-of-attack, deep-stall trim condition. Other aspects of the aerodynamic characteristics studied include the following: flow-visualization study, effect of negative angles of attack, lateral-directional characteristics, and comparison of the stall characteristics with another canard configuration.

17. Key Words (Suggested by Author(s))	18. Distribution Statement
Canard Power effects Stall characteristics Center-of-gravity locations Deep stall General aviation High angle of attack Longitudinal and lateral-directional stability and control Flow visualization Wind-tunnel test	Unclassified - Unlimited Subject Category 05

19. Security Classif. (of this report)	20. Security Classif. (of this page)	21. No. of Pages	22. Price
Unclassified	Unclassified	46	A03

For sale by the National Technical Information Service, Springfield, Virginia 22161

NASA-Langley, 1984